

# Dark halo response and the stellar initial mass function in early-type and late-type galaxies

Aaron A. Dutton<sup>1\*†</sup>, Charlie Conroy<sup>2</sup>, Frank C. van den Bosch<sup>3</sup>, Luc Simard<sup>4</sup>,  
J. Trevor Mendel<sup>1</sup>, Stéphane Courteau<sup>5</sup>, Avishai Dekel<sup>6</sup>, Surhud More<sup>7</sup>,  
& Francisco Prada<sup>8</sup>

<sup>1</sup>*Dept. of Physics and Astronomy, University of Victoria, Victoria, BC, V8P 5C2, Canada.*

<sup>2</sup>*Harvard-Smithsonian Center for Astrophysics, Cambridge, MA, USA.*

<sup>3</sup>*Astronomy Department, Yale University, P.O. Box 208101, New Haven, CT 06520-8101, USA.*

<sup>4</sup>*Herzberg Institute of Astrophysics, National Research Council of Canada, 5071 West Saanich Road, Victoria, B.C., V9E 2E7, Canada.*

<sup>5</sup>*Department of Physics, Engineering Physics & Astronomy, Queen's University, Kingston, Ontario, Canada.*

<sup>6</sup>*Racah Institute of Physics, The Hebrew University, Jerusalem 91904, Israel.*

<sup>7</sup>*Kavli Institute for Cosmological Physics, University of Chicago, 933 East 56th Street, Chicago, IL 60637, USA.*

<sup>8</sup>*Instituto de Astrofísica de Andalucía (CSIC), E18008 Granada, Spain.*

accepted to MNRAS

## ABSTRACT

We investigate the origin of the relations between stellar mass and optical circular velocity for early-type (ETG) and late-type (LTG) galaxies — the Faber-Jackson (FJ) and Tully-Fisher (TF) relations. We combine measurements of dark halo masses (from satellite kinematics and weak lensing), and the distribution of baryons in galaxies (from a new compilation of galaxy scaling relations), with constraints on dark halo structure from cosmological simulations. The principle unknowns are the halo response to galaxy formation and the stellar initial mass function (IMF). The slopes of the TF and FJ relations are naturally reproduced for a wide range of halo response and IMFs. However, models with a universal IMF and universal halo response cannot *simultaneously* reproduce the zero points of both the TF and FJ relations. For a model with a universal Chabrier IMF, LTGs require halo expansion, while ETGs require halo contraction. A Salpeter IMF is permitted for high mass ( $\sigma \gtrsim 180 \text{ km s}^{-1}$ ) ETGs, but is inconsistent for intermediate masses, unless  $V_{\text{circ}}(R_e)/\sigma_e \gtrsim 1.6$ . If the IMF is universal and close to Chabrier, we speculate that the presence of a major merger may be responsible for the contraction in ETGs while clumpy accreting streams and/or feedback leads to expansion in LTGs. Alternatively, a recently proposed variation in the IMF disfavors halo contraction in both types of galaxies. Finally we show that our models naturally reproduce flat and featureless circular velocity profiles within the optical regions of galaxies without fine-tuning.

**Key words:** dark matter – galaxies: fundamental parameters – galaxies: structure – galaxies: haloes – galaxies: spiral – galaxies: elliptical lenticular, cD

## 1 INTRODUCTION

Galaxy properties obey several fundamental relations, which have long been thought to hold important clues about the physical processes that influenced their formation and evolution. The relations between rotation velocity and luminosity (for late-types) and velocity dispersion and luminosity

(for early-types) are particularly interesting as they connect luminous mass with dynamical mass (which includes not only baryons but also dark matter). These relations are also known as the Tully-Fisher (Tully & Fisher 1977) and Faber-Jackson (Faber & Jackson 1976) relations.

The scatter in these relations is small, 0.07 dex in velocity for FJ (e.g., Gallazzi et al. 2006) and 0.05 dex in velocity for TF (e.g., Courteau et al. 2007b; Pizagno et al. 2007), which has enabled these relations to be used as secondary distance indicators. The smallness and source of the scatter

\* dutton@uvic.ca

† CITA National Fellow

is also interesting from a galaxy formation point of view. For early-type galaxies the scatter in velocity dispersion correlates with galaxy size, or surface brightness. This leads to the so-called fundamental plane of early-type galaxies, a correlation between size, surface brightness and velocity dispersion (Dressler et al. 1987; Djorgovski & Davis 1987). By contrast the scatter in the TF relation is independent of size or surface brightness (Zwaan et al. 1995; Courteau & Rix 1999; Courteau et al. 2007b; Pizagno et al. 2007), suggesting that the TF relation is the edge on projection of the fundamental plane for late-type galaxies.

The origin of these scaling relations in  $\Lambda$ CDM cosmologies is typically thought to be the relation between halo virial velocity and virial mass, which scale as  $V_{\text{vir}} \propto M_{\text{vir}}^{1/3}$ . Accounting for the higher halo concentrations in lower mass dark matter haloes results in a shallower slope for the relation between the maximum circular velocity of dark matter haloes and the halo virial mass:  $V_{\text{max,h}} \propto M_{\text{vir}}^{0.29}$  (Bullock et al. 2001). This scaling is similar to the observed stellar mass TF and FJ relations:  $\sigma_e \propto M_{\text{star}}^{0.29}$  (Gallazzi et al. 2006) and  $V_{2.2} \propto M_{\text{star}}^{0.28}$  (Dutton et al. 2010b), where  $\sigma_e$  is the velocity dispersion within the half-light radius, and  $V_{2.2}$  is the rotation velocity at 2.2 disk scale lengths. In what follows we define  $V_{\text{opt}} = V_{2.2}$  for late-types, and  $V_{\text{opt}} \propto \sigma_e$  for early-types. However, for the  $V_{\text{max,h}} - M_{\text{vir}}$  relation to be the direct origin of the TF and FJ relations requires that  $V_{\text{opt}}/V_{\text{max,h}}$ , and  $M_{\text{star}}/M_{\text{vir}}$  are constants. In Dutton et al. (2010b) we showed that this is at best only approximately the case. The relation between  $V_{\text{opt}}$  and  $V_{\text{vir}}$  depends on three factors: 1) The contribution of baryons to  $V_{\text{opt}}$ ; 2) The structure of the “pristine” dark matter halo (i.e., without the influence of baryons); and 3) The response of the dark matter halo to galaxy formation.

For low mass star-forming galaxies gas dominates their baryonic budget, but for high mass star-forming galaxies and most non star-forming galaxies, stars dominate the baryon budget. A key uncertainty in measuring stellar masses is the stellar initial mass function (IMF). There is a factor of  $\sim 2$  difference between the masses derived assuming the traditional Salpeter (1955) IMF compared with those derived assuming a Chabrier (2003) or Kroupa (2001) IMF. These latter IMFs are based on more recent measurements in the solar neighbourhood.

The structure of “pristine” dark matter haloes, has been extensively studied using cosmological N-body simulations (e.g., Navarro, Frenk, & White 1996a; Navarro, Frenk, & White 1997; Bullock et al. 2001; Eke, Navarro & Steinmetz 2001; Zhao et al. 2003; Navarro et al. 2004; Diemand et al. 2005, 2007; Macciò et al. 2007; Neto et al. 2007; Macciò et al. 2008; Zhao et al. 2009; Navarro et al. 2010; Klypin et al. 2010; Muñoz-Cuartas et al. 2011). While the nature of the density profile in the inner 0.1% of the virial radius is still uncertain, and the three parameter Einasto profile provides better fits than the broken power law of Navarro, Frenk, & White (1997, hereafter NFW), (Merritt et al. 2006), on the scales relevant for modeling galaxy kinematics  $\Lambda$ CDM dark matter haloes are well described by the two parameter NFW function. These two parameters are correlated with small scatter, such that the structure of dark matter haloes is almost completely determined by their mass.

The response of the halo to galaxy formation has traditionally been modeled assuming galaxy formation is adi-

abatic, i.e., changes in potential are slow compared to the dynamical time. Under this assumption the halo is expected to contract, resulting in so-called adiabatic contraction (Blumenthal et al. 1986). The standard model assumes dark halo particles are on circular orbits. Using more realistic orbits results in weaker halo contraction (Wilson 2003; Gnedin et al. 2004; Sellwood & McGaugh 2005). Recent hydrodynamical simulations of galaxy formation yield even weaker halo contraction (Abadi et al. 2010; Duffy et al. 2010; Pedrosa et al. 2010; Tissera et al. 2010). If galaxy formation is adiabatic, then the halo response should depend only on the final distribution of the baryons, and not on the assembly history. In these simulations the assembly history does matter, and thus this calls into question the basic assumption that halo response to galaxy formation is adiabatic.

It is also possible for haloes to expand in response to galaxy formation, via a number of processes: rapid mass loss from the galaxy, e.g., driven by supernovae (Navarro, Eke, & Frenk 1996b; Gnedin & Zhao 2002; Read & Gilmore 2005; Governato et al. 2010); dynamical friction operating on baryonic clumps (El-Zant, Shlosman & Hoffman 2001; El-Zant et al. 2004; Elmegreen et al. 2008; Jardel & Sellwood 2009) or galactic bars (Weinberg & Katz 2002; Holley-Bockelmann et al. 2005; Sellwood 2008). Thus while the underlying structure of dark matter haloes is well understood, in order to understand the origin of the TF and FJ relations, it is necessary to know the stellar IMF, and how dark matter haloes respond to galaxy formation.

Upper limits to stellar mass-to-light ratios, and hence the IMF, can be obtained from galaxy dynamics. For spiral galaxies, a Salpeter IMF is ruled out from maximal disk fits to resolved rotation curves (Bell & de Jong 2001). An IMF with stellar masses 0.15 dex lower than a Salpeter, the so-called diet-Salpeter IMF, is the upper limit. For elliptical galaxies a Salpeter IMF is also ruled out for some galaxies (Cappellari et al. 2006). But massive elliptical galaxies ( $\sigma > 200 \text{ km s}^{-1}$ ) are consistent with a Salpeter IMF (Bernardi et al. 2010), which may even be favored over lighter IMFs (Treu et al. 2010; Auger et al. 2010a). An alternative constraint on the stellar IMF comes from choosing the stellar mass-to-light ratio normalization that minimizes the scatter in the baryonic<sup>1</sup> TF relation (Stark, McGaugh, Swaters 2009). This favours a diet-Salpeter IMF with an uncertainty of  $\pm 0.1$  dex in the stellar mass-to-light ratio.

For a Chabrier IMF, elliptical galaxies require halo contraction to explain the mass discrepancy between the observed dynamical masses and those predicted when galaxies are embedded in NFW haloes (Schulz et al. 2010; Tollerud et al. 2011). However, for late-type galaxies, models with halo contraction over-predict the rotation velocities at fixed luminosity or stellar mass (Dutton et al. 2007; Dutton & van den Bosch 2009; Trujillo-Gomez et al. 2010).

In this paper we construct bulge-disk-halo models of early-type and late-type galaxies. These models are constrained to reproduce the distribution of stars and gas in galaxies, the relation between stellar mass and halo mass, and the structure of dark matter haloes in cosmological simulations. The key unknowns are the stellar IMF and the halo

<sup>1</sup> The baryonic TF relation is the relation between rotation velocity and baryonic mass (i.e., stars plus cold gas).

response to galaxy formation. We use the observed TF and FJ relations to place constraints on these two unknowns. As a by-product of this exercise, we measure the average dark matter fractions within the optical regions of early-type and late-type galaxies as a function of stellar mass.

This paper is organized as follows. In §2 we describe the mass models. In §3 we discuss the observational constraints. In §4 we present model TF and FJ relations and compare to the observations. A discussion is given in §5 and a summary in §6.

## 2 MASS MODELS

This section describes the mass models that we construct to compare to the observed scaling relations. The mass models consist of 3 components for early-types (stellar bulge, stellar disk, and dark matter halo), and 4 components for late-types (stellar bulge, stellar disk, gas disk, and dark matter halo). The circular velocity at radius,  $r$ , in the plane of the disk is given by the quadratic sum of the circular velocities of the various components:

$$V(r) = \sqrt{V_b^2(r) + V_d^2(r) + V_g^2(r) + V_h^2(r)}, \quad (1)$$

where the subscripts, b, d, g, and h, refer to the stellar bulge, stellar disk, gas disk, and dark matter halo, respectively.

### 2.1 Baryons

We model the stellar bulge with a Hernquist profile (Hernquist 1990)

$$\rho(r) = \frac{M_b}{2\pi} \frac{r_h}{r(r+r_h)^3}, \quad (2)$$

where  $M_b$  is the bulge mass, and  $r_h$  is a scale radius. We adopt the Hernquist profile as it provides a convenient analytical approximation to the de-projected de Vaucouleurs profile, which is the assumed profile in our bulge plus disk fits (see § 3.1). The projected half mass radius is given by  $R_{50b} = 1.815r_h$ . The enclosed mass of a Hernquist sphere is given by

$$M_b(r) = M_b \frac{r^2}{(r+r_h)^2}, \quad (3)$$

and the circular velocity is given by

$$V_b(r) = \sqrt{GM_b \frac{r}{(r+r_h)^2}}. \quad (4)$$

We model the stellar disk with an exponential surface density profile

$$\Sigma_d(R) = \frac{M_d}{2\pi R_d^2} \exp(-R/R_d), \quad (5)$$

which is specified by two parameters: the disk mass  $M_d$  and disk scale length  $R_d$ . The half mass radius of the disk is given by  $R_{50d} = 1.678R_d$ . For late-type galaxies we include a gas disk which we also model with an exponential profile

$$\Sigma_g(R) = \frac{M_g}{2\pi R_g^2} \exp(-R/R_g), \quad (6)$$

which is specified by two parameters: the gas mass  $M_g$  and gas disk scale length  $R_g$ .

For late-type galaxies we assume the stellar disks are infinitesimally thin. The circular velocity at radius,  $r$ , (in the plane of the disk) of a thin exponential disk of mass  $M_d$  and scale length  $R_d$  is given by:

$$V_d^2(r) = \frac{GM_d}{R_d} 2y^2 [I_0(y)K_0(y) - I_1(y)K_1(y)], \quad (7)$$

where  $y = r/(2R_d)$ , and  $I_n$  and  $K_n$  are modified Bessel functions (Freeman 1970).

For early-type galaxies the “disk” (i.e., the exponential) component that we fit to the observed photometry is usually not a true disk (see § 3.1). Thus in our dynamical models for early-types we assume the exponential component is spherical. In this case the 3D density profile is given by (e.g., van den Bosch & de Zeeuw 1996)

$$\rho(r) = \rho_{0,d} K_0(r/R_d), \quad (8)$$

where  $\rho_{0,d} = M_d/(2\pi^2 R_d^3)$ , and  $K_0$  is a modified Bessel function. We then obtain the circular velocity by integrating Eq. 8.

### 2.2 Dark matter

For the dark matter halo, we use a spherical NFW (Navarro, Frenk, & White 1997) profile

$$\rho(r) = \frac{\delta_c \rho_{\text{crit}}}{(r/r_{-2})(1+r/r_{-2})^2}. \quad (9)$$

Here  $r_{-2}$  is the radius where the logarithmic slope of the density profile is  $-2$ ,  $\rho_{\text{crit}}$  is the critical density of the universe, and  $\delta_c$  is the characteristic halo density. We reparametrize the halo by the virial mass,  $M_{200}$  and the concentration  $c = R_{200}/r_{-2}$ , where  $R_{200}$  is the virial radius. We adopt the definition of the virial mass such that the average density inside the virial radius is equal to 200 times the critical density of the universe. Thus, for a given  $M_{200}$ , the virial radius and circular velocity at the virial radius,  $V_{200}$  are related to each other at redshift  $z = 0$  by:

$$\frac{R_{200}}{(h^{-1}\text{kpc})} = \frac{V_{200}}{(\text{km s}^{-1})} = \left[ G \frac{M_{200}}{(h^{-1}M_\odot)} \right]^{1/3}, \quad (10)$$

where  $G \simeq 4.301 \times 10^{-6} \text{ km}^2 \text{ s}^{-2} \text{ kpc } M_\odot^{-1}$ . The mass enclosed within a spherical radius,  $r$ , is given by

$$M(r) = M_{200} A(r/r_{-2})/A(c), \quad (11)$$

where  $A(x) = \ln(1+x) - x/(1+x)$ . And thus the circular velocity at radius,  $r$ , is given by

$$V_h(r) = V_{200} \sqrt{\frac{A(r/r_{-2})}{r/r_{-2}} \frac{c}{A(c)}}. \quad (12)$$

#### 2.2.1 dark matter halo response to galaxy formation

The process of galaxy formation is expected to modify the pristine dark matter density profile. If galaxy formation is a slow and smooth process then the halo is expected to contract (e.g., Blumenthal et al. 1986; Gnedin et al. 2004; Sellwood & McGaugh 2005). However, if the initial stages of galaxy formation involve the mergers of massive clumps of gas, dynamical friction between the baryons and dark matter may result in net halo expansion (e.g., El-Zant et al. 2001). In addition other processes such as rapid ejection of baryons

from the disk through supernova driven winds (e.g., Navarro et al. 1996b), and galactic bars (Weinberg & Katz 2002) may also contribute to expanding the halo.

In the standard formalism the adiabatic invariant is  $rM(r)$ , and thus

$$r_f/r_i = M_i(r_i)/M_f(r_f), \quad (13)$$

where  $M_i(r)$  and  $M_f(r)$  are the initial and final mass distributions, and  $r_i$  and  $r_f$  are initial and final radii. Assuming no shell crossing of the dark matter,  $M_{h,i}(r_i) = M_{h,f}(r_f)$ , and that baryons initially follow the same mass profile as the dark matter,  $M_{b,i}(r_i) = m_{\text{gal}}M_{h,i}(r_i)$ , then

$$r_f/r_i = M_{h,i}(r_i)/[M_{b,f}(r_f) + (1 - m_{\text{gal}})M_{h,i}(r_i)], \quad (14)$$

where  $M_{b,f}$  is the final mass distribution of the baryons, and  $m_{\text{gal}}$  is the baryon mass fraction. For our mass models we know  $M_{b,f}(r)$ ,  $M_i(r)$ , and  $m_{\text{gal}}$ , and thus one can solve Eq. 14 for the mapping between  $r_i$  and  $r_f$ .

Using cosmological hydrodynamical simulations of galaxy clusters, Gnedin et al. (2004) advocate a modified adiabatic invariant  $rM(< \bar{r})$ , where  $\bar{r}/R_{200} = 0.85(r/R_{200})^{0.8}$ , and thus

$$r_f/r_i = M_i(\bar{r}_i)/M_f(\bar{r}_f). \quad (15)$$

This formula results in slightly less contraction than the standard formula (Eq. 13).

More recent cosmological hydrodynamical simulations of galaxies (Abadi et al. 2010; Pedrosa et al. 2010; Tissera et al. 2010) have found less contraction than predicted by the Blumenthal et al. (1986) and Gnedin et al. (2004) models. Abadi et al. (2010) advocate the following formula

$$r_f/r_i = 1 + 0.3[(M_i(r_i)/M_f(r_f))^2 - 1]. \quad (16)$$

In order to explore the possibility of expansion we also consider the generalized contraction formula from Dutton et al. (2007). A modified contraction parameter  $\Gamma$  can be defined as

$$\Gamma = (r_f/r_i)^\nu. \quad (17)$$

For  $\nu = 1$ , we have the standard Blumenthal et al. (1986) contraction formula (Eq. 13), if  $\nu = 0$  there is no contraction, and if  $\nu < 0$  there is expansion. The Gnedin et al. (2004) model can be well approximated with  $\nu = 0.8$ , while the Abadi et al. (2010) model corresponds to  $\nu \sim 0.4$ .

### 3 CONSTRAINTS

In this section we discuss the observational and theoretical constraints to our mass models. Readers that are interested in the results of our mass models, but not the details of the constraints, may skip to § 3.12.

Here we present new determinations of the structural and dynamical scaling relations of early-type and late-type galaxies. We use both new measurements as well as data compiled from the literature. We start with a discussion of the scaling relations derived from Sloan Digital Sky Survey (SDSS; York et al. 2000) data release seven (DR7) (Abazajian et al. 2009), and then proceed to other observational constraints.

The main use for the observed structural scaling relations we present is to enable a determination of the average

mass of baryons (i.e., stars and gas), within a specified radius, as a function of the stellar mass of a galaxy. These scaling relations are also of interest in their own right as constraints to cosmological galaxy formation models.

#### 3.1 General properties of the SDSS sample

A number of the scaling relations we present here are based on a large sample of galaxies from the SDSS/DR7. Structural properties are derived from two component fits (nominally referred to as bulge and disk) on SDSS  $g$ - and  $r$ -band images performed using GIM2D (Simard et al. 2002; Simard et al. , in prep). The two components are special cases of the Sérsic function

$$\Sigma(R) = \Sigma_0 \exp[-(R/R_0)^{1/n}], \quad (18)$$

which is characterized by the Sérsic index,  $n$ . Bulges are modeled as elliptical Sérsic  $n = 4$  profiles (i.e., de Vaucouleurs) with axis ratio  $q_b$ , while disks are modeled as elliptical Sérsic  $n = 1$  profiles (i.e., exponential) with axis ratio  $q_d$ . The 2D models are convolved with the point spread function due to seeing, and fitted to the observed images using a Monte Carlo Markov Chain technique.

Rest frame  $g$  and  $r$  magnitudes have been derived from GIM2D model magnitudes with a  $k$ -correction to  $z = 0$  based on SDSS petrosian  $ugriz$  magnitudes. Stellar masses are from the MPA/JHU group<sup>2</sup>, who fit SDSS  $ugriz$  model magnitudes with Bruzual & Charlot (2003) stellar population synthesis models, and adopting a Chabrier (2003) IMF. Our full sample consists of  $\sim 655\,000$  galaxies with spectroscopic redshifts, GIM2D fits and stellar masses. We prune this down to  $\sim 170\,000$  early-type and  $\sim 100\,000$  late-type galaxies using a number of cuts as described below.

- **Redshift Range:**  $0.005 \leq z \leq 0.2$ . This leaves  $\sim 614\,000$  galaxies, or  $\sim 94\%$  of the sample.

- **Color Cuts:** We split galaxies into red (early-types) and blue (late-types) based on the bimodality in the  $(g-r)$  color-stellar mass plane (Fig. 1). As a separator we adopt

$$(g-r) = 0.59 + 0.052[\log_{10}(M_{\text{star}}/M_\odot) - 10], \quad (19)$$

which is shown as solid green vertical lines in Fig. 1. This results in  $\sim 246\,000$  late-type galaxies and  $\sim 368\,000$  early-type galaxies.

- **Stellar Mass Limit:**  $M_{\text{min}} = 10^{10.2}M_\odot[(z/0.1)^2 + 0.2(z/0.1)^4]$  for late-type galaxies, and a factor of 2 higher for early-type galaxies. This removes the color bias towards bluer galaxies in the  $(g-r)$ - stellar mass plane caused by the  $r$ -band magnitude limit for SDSS spectroscopy (see Appendix A in van den Bosch et al. 2008 for a discussion of this bias). This selection leaves  $\sim 150\,000$  late-type galaxies (61% that passed the redshift cut) and  $\sim 255\,000$  early-type galaxies (69% that passed the redshift cut).

- **Disk Axis Ratio Cut:**  $b/a > 0.5$ . For thin disks this corresponds to an inclination of less than 60 degrees. This reduces contamination of the red sequence with dust reddened late-types, and reduces extinction biases to the structural parameters. This selection leaves  $\sim 106\,000$  late-type galaxies (71% that passed mass and redshift cuts) and

<sup>2</sup> Available at <http://www.mpa-garching.mpg.de/SDSS/DR7/>

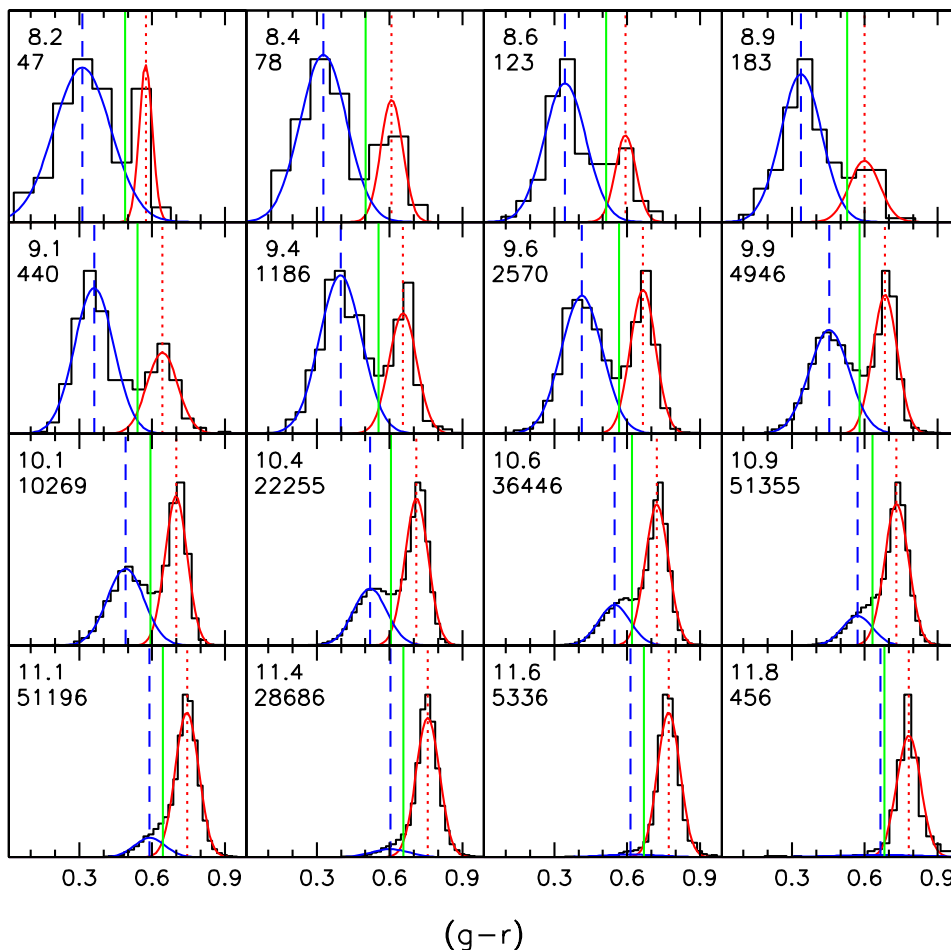


**Figure 1.** Histograms of  $(g-r)$  color in bins of stellar mass for galaxies that meet our redshift, minimum stellar mass and disk axis ratio cuts. The mean of  $\log_{10}(M_{\text{star}}/M_{\odot})$  and the number of galaxies are indicated at the top left corner of each panel. Galaxies have been separated into red and blue using a Monte Carlo method that assigns color based on double Gaussian fits to the galaxy color distribution in each mass bin. The mean colors of the red and blue galaxies are shown as red dotted and blue dashed vertical lines. The separator between red and blue galaxies (Eq. 19) that we use for the rest of this paper is given by the solid green vertical lines.

$\sim 168\,000$  early-type galaxies (66% that passed mass and redshift cuts).

- **Stellar Velocity Dispersion:** For early-type galaxies we also require a stellar velocity dispersion from the SDSS/DR7 pipeline. This requires that the spectrum has been classified as an early-type. This selection leaves  $\sim 136\,000$  early-type galaxies (81% that passed previous cuts).

### 3.1.1 Interpretation of bulge-disk fits

How robust are our bulge-disk fits? For late-type galaxies it is well known that bulges are often better fit with Sérsic indices of  $n \sim 1 - 2$  (e.g., Courteau et al. 1996), rather than the  $n = 4$  that we adopt here. However, since the bulge half-light radii are typically much smaller than the radii at which we measure the rotation velocity (2.2 disk scale lengths), the structure of the bulge is not critical. What matters for our purposes is that the bulge-disk fits provide an accurate measurement of the *total* light within 2.2 disk scale lengths. We also do not attempt to distinguish between classical bulges, pseudo bulges and bars. Firstly, because

this is an unnecessary complication, and secondly because for typical galaxies (at redshifts  $z \gtrsim 0.1$ ) in our sample the  $\sim 1.5$  arcsec resolution of the SDSS imaging is not capable of distinguishing between these components.

The distribution of bulge and disk axis ratios gives an important diagnostic to the physical interpretation of our bulge and disk components, as these components are expected to have different distributions. For disks, the observed distribution should be uniform, with a cut off at low axis ratios corresponding to the finite thickness of galaxy disks, and a deficit of perfectly round galaxies due to spiral arms. For elliptical galaxies the distribution is expected to be skewed towards high axis ratios.

Fig. 2 shows distribution of axis ratios for  $n = 4$  components (“bulges”, red lines) and  $n = 1$  components (“disks”, blue lines) as a function of stellar mass, and the fraction of light in the  $n = 4$  component, hereafter the de Vaucouleurs fraction,  $f_{\text{deV}}$ <sup>3</sup>. We use galaxies that meet our redshift cut

<sup>3</sup> Note that our parameter  $f_{\text{deV}}$  should not be confused with the SDSS parameter  $\text{fracDev}$ . While both parameters measure the

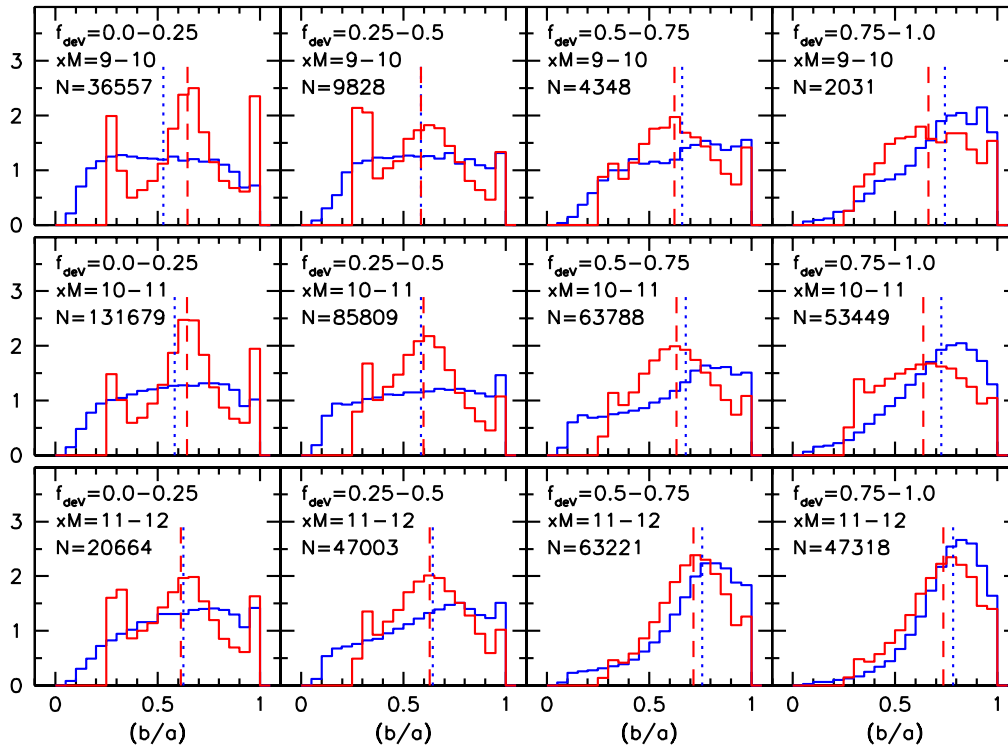


**Figure 2.** Axis ratio distributions of  $n = 4$  components “bulges” (red) and  $n = 1$  components “disks” (blue) for different stellar masses,  $xM \equiv \log_{10}(M_{\text{star}}/M_{\odot})$ , and de Vaucouleurs fractions,  $f_{\text{dev}}$ , for galaxies that meet our redshift cuts and redshift dependent stellar mass limit (based on early-type galaxies). The vertical lines show the median axis ratio for  $n = 4$  components (dashed) and  $n = 1$  components (dotted). For thin disks the distribution of axis ratios is uniform. This figure shows that the  $n = 1$  components in galaxies with low  $f_{\text{dev}}$  are disks, whereas the  $n = 1$  components in galaxies with high  $f_{\text{dev}}$  are spheroids. The value of  $f_{\text{dev}}$  above which the  $n = 1$  components are predominantly spheroids decreases with increasing stellar mass.

and redshift dependent stellar mass limit (based on early-type galaxies). For galaxies with  $f_{\text{dev}} < 0.25$  (far left panels) the observed distribution of disk axis ratios is as expected. But for galaxies with  $f_{\text{dev}} > 0.75$  (far right panels) the observed distribution of disk axis ratios is skewed towards high values, indicating that these  $n = 1$  components are in fact spheroids. The value of  $f_{\text{dev}}$  above which the  $n = 1$  components are predominantly spheroids decreases with increasing stellar mass. For example, for low stellar mass galaxies, the transition is at  $f_{\text{dev}} \simeq 0.75$ , whereas for high stellar mass galaxies the transition is at  $f_{\text{dev}} \simeq 0.5$ .

These results should not be considered a surprise, as while the average Sérsic index of elliptical galaxies is  $n \simeq 4$ , it is known that in general  $n \neq 4$ . The mean Sérsic index of elliptical galaxies increases with increasing luminosity (e.g., Prugiel & Simien 1997; Graham & Guzman 2003; Ferrarese et al. 2006; Kormendy et al. 2009). In particular high luminosity ellipticals have  $n > 4$ , and thus will be better fitted by a model with an  $n = 4$  plus an  $n = 1$  component rather than just a single  $n = 4$  component.

Based on these results, we assume that the majority of the  $n = 1$  components in our fits to early-type galaxies are not true disks. Thus in our dynamical models for early-type

fraction of the light in an  $n = 4$  component, they are calculated using different methods, with our method being more robust than that used by SDSS.

galaxies we assume that the  $n = 1$  components are spherical. There are differences between the circular velocity profiles of a thin disk and a sphere of the same projected mass profile, with thin disks having 10-15% higher maximum circular velocities (Binney & Tremaine 1987). However, for early-type galaxies the  $n = 4$  component dominates the baryons within the half-light radius, so the exact details for how one models the 3D structure of the  $n = 1$  component is not critical to the conclusions of this paper.

### 3.2 Comparison between stellar mass estimates

In this paper we use stellar masses estimated using two different methods: The relations between optical color and stellar mass-to-light ratio from Bell et al. (2003),  $M_{\text{Bell}}$ ; and from *ugriz* spectral energy distribution (SED) fitting from the MPA/JHU group,  $M_{\text{MPA}}$ . The MPA/JHU masses have been explicitly calculated with a Chabrier IMF. We have subtracted 0.1 dex from the Bell et al. (2003) masses, so that these correspond to those from a Salpeter IMF -0.25 dex, and hence a Chabrier IMF. Thus both of the mass estimates we use nominally correspond to a Chabrier (2003) IMF.

Here we measure the differences between these masses, so that scaling relations based on either of these methods can be more directly compared. Fig. 3 shows that the scatter between the two different masses is small ( $\lesssim 0.1$  dex), and at

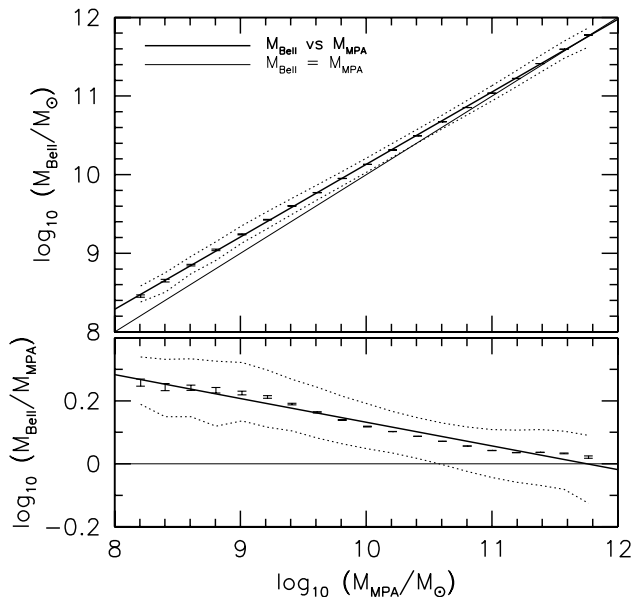


**Figure 3.** Comparison between stellar masses from the MPA/JHU group,  $M_{\text{MPA}}$ , and those derived from the  $(g-r)$  -  $M_{\text{star}}/L_r$  relation in Bell et al. (2003),  $M_{\text{Bell}}$ . We have subtracted 0.1 dex from the Bell et al. (2003) formula, so that  $M_{\text{Bell}}$  and  $M_{\text{MPA}}$  both nominally correspond to a Chabrier (2003) IMF. The error bars show the error on the median, while the dotted lines show the 16th and 84th percentiles. The solid line gives our fitting formula Eq. 20.

high masses the two methods agree, but there is a systematic difference that increases with decreasing mass. We fit the relation between the two masses using the following power law

$$\log_{10} \left( \frac{M_{\text{Bell}}}{10^{10} M_{\odot}} \right) = 0.130 + 0.922 \log_{10} \left( \frac{M_{\text{MPA}}}{10^{10} M_{\odot}} \right). \quad (20)$$

Similar differences between masses from Bell et al. (2003) and masses from Blanton & Roweis (2007) were shown by Li & White (2009). The masses from Blanton & Roweis (2007) use a similar methodology to those from the MPA/JHU group, so the good correspondence is expected.

Both the MPA/JHU and Bell et al. (2003) masses are based on SED fits to SDSS photometry, but there are a number of possible sources of the systematic differences between the MPA/JHU and Bell et al. (2003) masses, which we briefly list here. 1) Curvature in color-M/L relation at blue colors (e.g., Portinari et al. 2004). 2) Different treatments for extinction (MPA/JHU apply an extinction correction, Bell et al. does not). 3) Different methods for deriving stellar masses from an SED. 4) Different stellar population synthesis (SPS) codes: Bruzual & Charlot (2003) vs PEGASE (Fioc & Rocca-Volmerange 1997).

Since the MPA/JHU masses are more direct measurements, throughout this paper we adopt these as our fiducial masses. All scaling relations presented or used in this paper use MPA/JHU masses directly, or Bell et al. (2003) masses converted to MPA/JHU masses using Eq. 20.

**Table 1.** Parameters of double power-law fitting formula (Eq. 21) to the  $y = R_{50}/[\text{kpc}]$  vs  $x = M_{\text{star}}/M_{\odot}$  relations in Fig. 4.

Component	$\alpha$	$\beta$	$\log_{10} M_0$	$\log_{10} R_0$	$\gamma$
Late-types					
Disks $R_{50}$	0.20	0.46	10.39	0.75	1.95
Bulges $R_{50}$	0.17	0.35	11.02	0.51	2.8
Total $R_{50}$	0.21	0.47	10.86	0.84	2.2
Early-types					
Disks $R_{50c}$	0.27	0.59	9.97	0.32	1.5
Bulges $R_{50c}$	0.03	0.54	10.07	-0.07	4.3
Total $R_{50c}$	0.03	0.64	10.09	0.16	1.3

### 3.3 Size - stellar mass relations

Fig. 4 shows the size - stellar mass relations for early-type (right panel) and late-type (left panel) galaxies. The red, blue and black lines show the relations for the  $n = 4$  components,  $n = 1$  components, and total, respectively. The mass is always the total stellar mass, but the sizes are those of the separate components. For the late-type galaxies the sizes are the major-axis  $r$ -band half-light sizes,  $R_{50}$ . For the early-type galaxies the sizes are the circularized  $r$ -band half-light sizes,  $R_{50c} = \sqrt{q}R_{50}$ , where  $q$  is the luminosity weighted minor-to-major axis ratio of the galaxy ( $q = q_d f_d + q_b f_b$ ), and  $R_{50}$  is the major axis half-light size. Our use of major axis sizes for late-types and circularized sizes for early-types is motivated by our desire to construct dynamical models. For disk-dominated galaxies the major axis size is the only sensible size to use. For bulge-dominated galaxies the situation is more complicated due to the unknown intrinsic 3D shape. We use circularized sizes (i.e., intermediate axis) for early-type galaxies for two reasons: Firstly, in our dynamical models we assume that the bulges are spherical; Secondly, for an ellipsoidal mass profile, the potential is more spherical than the mass profile.

We fit the data using the following double power-law

$$y = y_0 \left( \frac{M_{\text{star}}}{M_0} \right)^{\alpha} \left[ \frac{1}{2} + \frac{1}{2} \left( \frac{M_{\text{star}}}{M_0} \right)^{\gamma} \right]^{(\beta - \alpha)/\gamma}, \quad (21)$$

with  $y = R_{50}$ . These fits are shown with solid lines in Fig. 4 and the parameters are given in Table 1.

For late-type galaxies the size-mass relation has a pronounced curvature, with a slope of 0.47 at high masses and 0.21 at low masses. Curvature in the half light radius - stellar mass relation for late-types (defined by having  $n < 2.5$ ) was measured by Shen et al. (2003). Their relation is shown by the long-dashed line. It has similar slopes at low and high masses, but a significantly lower zero-point. This difference can mostly be attributed to the fact that the sizes used by Shen et al. (2003) were performed using circular apertures, which biases the sizes of disk dominated galaxies low, on average by  $\simeq 0.15$  dex

For early-type galaxies the half-light radius stellar mass relation has a slope that ranges from  $\simeq 0$  at low masses to  $\simeq 0.6$  at high masses. Flattening of the slope at low luminosities has been reported previously (e.g., Graham & Guzman 2003; Graham & Worley 2008). At high masses our results are in good agreement with the power-law scaling from Shen et al. (2003), who found  $R_{50} \propto M_{\text{star}}^{0.56}$  for early-types

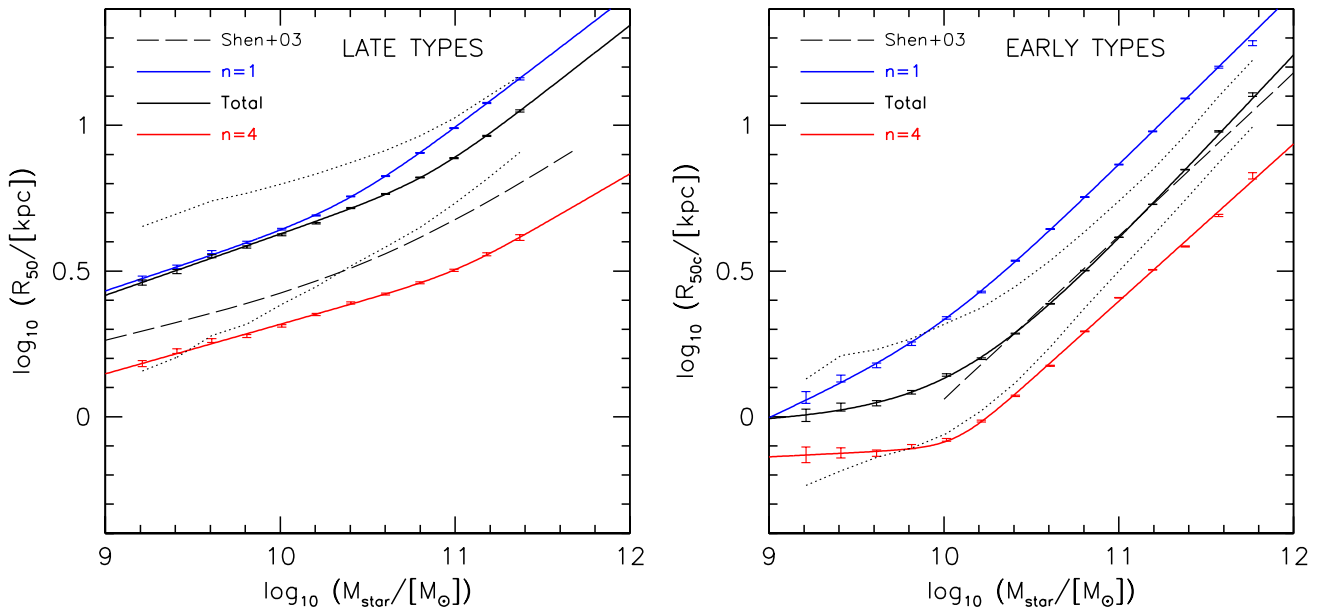


**Figure 4.** Size-stellar mass relations for late-type (left panel) and early-type (right panel) galaxies. For the early-type galaxies we show circularized half-light radii,  $R_{50c}$ , whereas for the late-type galaxies we show the major-axis half-light radii,  $R_{50}$ . In both panels the blue error bars show the median sizes of the disk (Sérsic  $n = 1$  component), the red error bars show the median sizes of the bulge (Sérsic  $n = 4$  component), and the black error bars show the median sizes of the whole galaxy. The solid lines show fits to these data using Eq. 21. The parameters of these fits are given in Table. 1. For comparison we show the circularized half-light radii for early-type ( $n > 2.5$ ) and late-type ( $n < 2.5$ ) galaxies from Shen et al. (2003). For early-types there is good agreement, but for late-types the sizes from Shen et al. (2003) are smaller by  $\simeq 0.15$  dex due to circularization. The dotted lines show the 16th and 84th percentiles for the total half-light sizes, which shows that the scatter in sizes decreases at higher masses.

(defined to have Sérsic index  $n > 2.5$ ) with stellar masses greater than  $\sim 10^{10} M_{\odot}$ . The absolute differences between our size - mass relation and that from Shen et al. (2003) are less than 10%.

### 3.3.1 Conversion from optical sizes to stellar mass sizes

In theoretical models of disk galaxy formation, disks form inside-out (e.g., Dutton et al. 2011). This results in color gradients, with progressively larger scale lengths when going from stellar mass to  $K$ -band light to  $B$ -band light. Observations of face-on disk galaxies yield  $B$ -band sizes that are  $\simeq 0.03$  dex larger than  $V$ -band sizes, and that are  $\simeq 0.06$  dex larger than  $R$ -band sizes (MacArthur et al. 2003).

Assuming that the disks are exponential in each pass-band, and a power-law relation between stellar mass-to-light ratio and color (e.g., Bell & de Jong 2001), then one can show that the stellar disk will also have an exponential stellar mass density profile, with a scale length,  $R_{d,*}$ , given by

$$R_{d,*} = R_{d,R} / [1 + 2.5b(1 - R_{d,R}/R_{d,B})], \quad (22)$$

where  $b$  is the slope of the relation between  $M_*/L_R$  and  $(B-R)$  color,  $R_{d,B}$  and  $R_{d,R}$  are the scale lengths of the disk in  $B$ - and  $R$ -bands respectively. Adopting  $b = 0.683$  (Bell et al. 2003), and  $R_{d,R}/R_{d,B} = 0.87$  implies  $R_{d,*} = 0.82R_{d,R}$ , and thus  $R_{d,*} = 0.76R_{d,V}$ . The rest frame disk scale lengths of galaxies in our SDSS sample are roughly  $V$ -band, so we apply this correction to our late-type galaxies. We don't ap-

ply any corrections to the sizes of late-type bulges, or to the sizes of early-type galaxies.

### 3.4 De Vaucouleurs fraction - stellar mass relation

Using the GIM2D two component fits as described above, we compute median de Vaucouleurs fractions,  $f_{deV}$ , in  $r$ -band light of early-type and late-type galaxies. These relations are shown in Fig. 5. For late-type galaxies the relation is fitted with the following equation:

$$f_{deV} = f_{deV2} + \frac{f_{deV1} - f_{deV2}}{1 + (M_{star}/M_0)^{\gamma}}. \quad (23)$$

Here  $f_{deV1}$  is the asymptotic de Vaucouleurs fraction at low masses,  $f_{deV2}$  is the asymptotic de Vaucouleurs fraction at high masses,  $M_0$  is the transition mass, and  $\gamma$  controls the sharpness of the transition. For early-type galaxies, we use Eq. 21 with  $\log_{10} y = f_{deV}$ . The parameters of the fits are given in Table 2.

As discussed in §3.1.1 for late-type galaxies, the  $n = 1$  component usually corresponds to a disk, while the  $n = 4$  component usually corresponds to a spheroid. Thus for late-type we refer to the de Vaucouleurs fractions as bulge fractions. The median bulge fractions are  $\sim 10\%$  for stellar masses below  $M_{star} \simeq 2 \times 10^{10} M_{\odot}$ . Above this mass scale the median bulge fractions increase rapidly with mass. These trends are qualitatively the same as those between global Sérsic index and stellar mass from Dutton (2009). In particular, our new results confirm the prevalence of



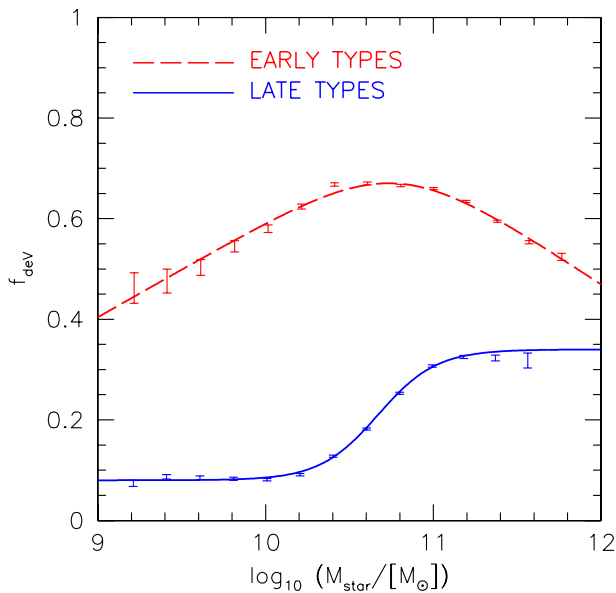


**Figure 5.** De Vaucouleurs fraction,  $f_{\text{dev}}$ , vs stellar mass,  $M_{\text{star}}$ , for early (red lines) and late-type (blue lines) galaxies. The de Vaucouleurs fraction is the fraction of  $r$ -band light in the Sérsic  $n = 4$  component, derived from two component ( $n = 4$ ,  $n = 1$ ) fits to the galaxy images. The error bars show the median and error on the median  $r$ -band bulge fraction in bins of width 0.2 dex in stellar mass. The lines show fits to these data points, using Eq. 23 with parameters given in Table 2.

**Table 2.** Parameters of fits to the de Vaucouleurs fraction - stellar mass relations for early-type and late-types galaxies in Fig. 5. For early-type galaxies we use Eq. 21 with  $\log_{10} y = f_{\text{dev}}$ . For late-type galaxies we use Eq. 23.

Late-type galaxies	$f_{\text{dev}1}$	$f_{\text{dev}2}$	$\log_{10} M_0$	$\gamma$	
	0.08	0.34	10.67	2.5	
Early-type galaxies	$\alpha$	$\beta$	$\log_{10} M_0$	$f_{\text{dev}0}$	$\gamma$
	0.19	-0.22	10.77	0.67	1.75

galaxies with low bulge fractions at stellar masses below  $M_{\text{star}} = 3 \times 10^{10} M_{\odot}$ .

As discussed in §3.1.1 for early-type galaxies the  $n = 1$  component does not always correspond to a physical disk, and thus the interpretation of  $f_{\text{dev}}$  in terms of bulges and disks is less straightforward. For our dynamical models our fiducial assumption is that the  $n = 1$  component in early-type galaxies is spherical.

### 3.5 The Tully-Fisher relation

The Tully-Fisher (TF) relation is the relation between rotation velocity (or linewidth) and luminosity (or stellar mass). Here we present a new determination of the stellar mass TF relation using data from Verheijen (2001) and Pizagno et al. (2007). As our velocity measure we adopt  $V_{2.2}$ : the rotation velocity measured at 2.2 disk scale lengths ( $R$ -band for the Verheijen sample and  $i$ -band for Pizagno et al. sam-

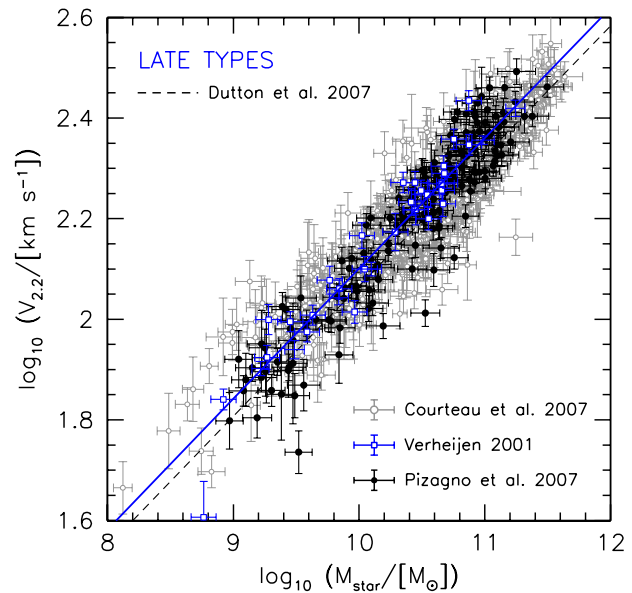


**Figure 6.** Tully-Fisher relation for spiral galaxies using data from Verheijen (2001); Pizagno et al. (2007) and Courteau et al. (2007b). The rotation velocity is measured at 2.2 disk scale lengths. The data is well fit by a power-law, as given by the solid blue line. This fit is in good agreement with that from Dutton et al. (2007) which was based on the Courteau et al. (2007b) sample. The small offset is due to a different stellar mass normalization.

ple). For the Verheijen (2001) galaxies we have computed  $V_{2.2}$  using disk scale lengths from McDonald, Courteau, & Tully (2009). Stellar masses were first calculated using the relations between color and stellar mass-to-light ratio from Bell et al. (2003), with an offset of -0.1 dex, corresponding to a Chabrier (2003) IMF, and then converted into the MPA/JHU masses using Eq. 20.

The TF data are shown in Fig. 6. The Verheijen (2001) galaxies are shown with blue symbols, the Pizagno et al. (2007) galaxies with black symbols. In grey we also show data from Courteau et al. (2007b). A fit to the Verheijen (2001) and Pizagno et al. (2007) galaxies (solid blue line in Fig. 6) is given by:

$$\log_{10} \left( \frac{V_{2.2}}{\text{km s}^{-1}} \right) = 2.179 + 0.259 \log_{10} \left( \frac{M_{\text{star}}}{10^{10.3} M_{\odot}} \right), \quad (24)$$

where the  $1\sigma$  uncertainty on the zero point is 0.005 and the  $1\sigma$  uncertainty on the slope is 0.01. We do not include the galaxies from Courteau et al. (2007) in this fit as this sample has a heterogeneous selection function. However, the data set compiled by Courteau et al. (2007b) has a TF relation (as calculated by Dutton et al. 2007, dashed line in Fig. 6) with a slope that is in good agreement with Eq. 24. The difference in zero point is explained by the different stellar mass normalizations used by Dutton et al. (2007) and this paper.

### 3.6 The Faber-Jackson relation

The Faber-Jackson (FJ) relation is the relation between velocity dispersion and luminosity (or stellar mass). Here we

present a new determination of the FJ relation for early-type galaxies using data from the SDSS. This sample has the same selection criteria as used for the early-type size-mass relation (Fig. 4).

As is common practice, we correct SDSS fiber velocity dispersions to velocity dispersions measured within the effective radius using the empirical calibration from Jorgensen et al. (1995). Since we wish to convert velocity dispersions to within  $R_e$  rather than  $R_e/8$  we use the quadratic formula from Jorgensen et al. (1995):

$$\log_{10} \frac{\sigma_{\text{ap}}}{\sigma_e} = -0.065 \log_{10} \left( \frac{R_{\text{ap}}}{R_e} \right) - 0.013 \left[ \log_{10} \left( \frac{R_{\text{ap}}}{R_e} \right) \right]^2, \quad (25)$$

where  $\sigma_{\text{ap}}$  is the velocity dispersion measured within the aperture radius,  $R_{\text{ap}}$ . For SDSS spectra  $R_{\text{ap}} = 1.5$  arcsec. The quadratic formula is more accurate than the more commonly used linear relation from Jorgensen et al. (1995):

$$\log_{10} \frac{\sigma_{\text{ap}}}{\sigma_e} = -0.04 \log_{10} \left( \frac{R_{\text{ap}}}{R_e} \right). \quad (26)$$

Using Eq. 25 results in average corrections that vary between  $0.00 \lesssim \log_{10}(\sigma_{\text{ap}}/\sigma_e) \lesssim 0.03$ , i.e., the velocity dispersion within  $R_e$  is smaller than the velocity dispersion with the SDSS aperture. The correction is approximately zero for stellar masses of  $\log_{10}(M_{\text{star}}/M_{\odot}) \simeq 10.4$ , and increases to lower and higher masses, reaching  $\simeq 0.015$  at  $\log_{10}(M_{\text{star}}/M_{\odot}) \simeq 9.5$  and  $\simeq 0.03$  at  $\log_{10}(M_{\text{star}}/M_{\odot}) \simeq 11.7$ . Since the aperture corrections to the velocity dispersion are small, they are not a significant source of systematic uncertainty.

The resulting FJ relation is shown in Fig. 7. The error bars show median velocity dispersions in bins of width 0.1 dex in stellar mass, while the dotted lines show the 16th and 84th percentiles of the distribution. We fit the FJ relation using Eq. 21 with  $y = \sigma_e$ , finding

$$\log_{10} \left( \frac{\sigma_e}{\text{km s}^{-1}} \right) = 2.23 + 0.37 \log_{10} \left( \frac{M_{\text{star}}}{10^{10.9} M_{\odot}} \right) - 0.19 \log_{10} \left[ \frac{1}{2} + \frac{1}{2} \left( \frac{M_{\text{star}}}{10^{10.9} M_{\odot}} \right) \right]. \quad (27)$$

The long-dashed line shows the FJ relation based on SDSS data from Gallazzi et al. (2006),

$$\log_{10} \left( \frac{\sigma_e}{\text{km s}^{-1}} \right) = 2.051 + 0.286 \log_{10} \left( \frac{M_{\text{star}}}{10^{10.3} M_{\odot}} \right), \quad (28)$$

who use the same IMF and velocity dispersion definition as used here. This power-law relation from Gallazzi et al. (2006) is in reasonable agreement with our measurements. There is, however, a curvature to our relation. Curvature at high and low stellar masses has been reported previously (e.g., Hopkins et al. 2008; Hyde & Bernardi 2009; Bernardi et al. 2011). In addition, curvature in the velocity dispersion - luminosity relation was hinted at by early studies (Tonry 1981; Davies et al. 1983), and is now firmly established (Matković & Guzman 2005). The short-dashed line shows the quadratic FJ relation from Hyde & Bernardi (2009). This agrees well with our measurements, except for a  $\simeq 0.04$  dex zero point offset which is due different definitions of velocity dispersion ( $\sigma_e$  vs  $\sigma_{e8}$ ).

At lower masses  $M_{\text{star}} \lesssim 10^{10} M_{\odot}$  the velocity dispersions are below  $80 \text{ km s}^{-1}$  and are subject to larger systematic uncertainties. However, none of our results are strongly

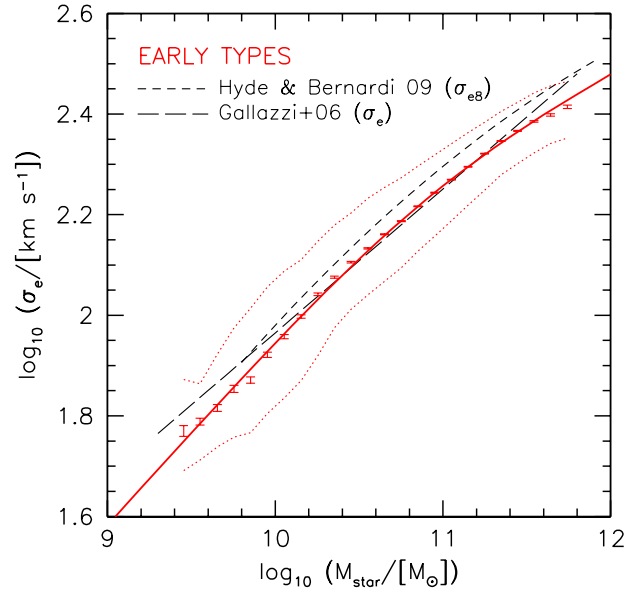


**Figure 7.** Velocity dispersion - stellar mass relation for early-type galaxies (also known as the Faber-Jackson relation). Velocity dispersions,  $\sigma_e$ , have been corrected to the effective radius. The dotted lines show the 16th and 84th percentiles of the distribution of  $\sigma_e$  at fixed mass. The error bars show the median and error on the median velocity dispersion in bins of width 0.1 dex in stellar mass. The solid line shows our double power-law fit to these data points, given in Eq. 27. The long-dashed line shows the power-law relation from Gallazzi et al. (2006), Eq. 28, which over-predicts the velocity dispersions at low and high masses. The short-dashed line shows the quadratic relation from Hyde & Bernardi (2009), which agrees well with our relation, except for a  $\simeq 0.04$  dex offset due to a different definition of velocity dispersion.

sensitive to whether we use the power-law FJ from Gallazzi et al. (2006; Eq. 28) or our double power-law fit using Eq 27 at low masses. We note that the deviations from power-laws of the  $\sigma_e - M_{\text{star}}$  and  $R_e - M_{\text{star}}$  relations are correlated: i.e., where  $\sigma_e$  is lower than the power-law fit,  $R_e$  is higher. Such a correlation is expected from the fundamental plane.

### 3.7 Converting velocity dispersions into circular velocities

In order to use the TF and FJ relations as dynamical constraints to our mass models, we need to convert velocity dispersions and rotation velocities into circular velocities (i.e., the rotation velocity of a massless test particle moving in a circular orbit). For late-type galaxies, we assume that the rotation velocity is equal to the circular velocity. This assumption is expected to be correct for galaxies with rotation velocities greater than about  $50 \text{ km s}^{-1}$ . For low mass galaxies pressure support from turbulence is expected to result in rotation velocities that are significantly lower than the circular velocities (e.g., Dalcanton & Stilp 2010).

Converting velocity dispersions into circular velocities is less straightforward. Based on the spherical Jeans equation, there is dependence on the density profile of the tracer population, the slope of the velocity dispersion profile, and the anisotropy parameter. Conversion factors motivated by

the Jeans equation that are used in the literature typically range from  $\sqrt{2}$  to  $\sqrt{3}$  (Courteau et al. 2007a).

In this section we use results and data from the literature to motivate a conversion factor between the velocity dispersion within the effective radius,  $\sigma(< R_e) \equiv \sigma_e$ , and circular velocity at the effective radius,  $V_{\text{circ}}(R_e)$ , of  $f = V_{\text{circ}}(R_e)/\sigma_e = 1.54^{+0.11}_{-0.10}$ , i.e., roughly half way between  $\sqrt{2}$  and  $\sqrt{3}$ .

We start our discussion with the result from Padmanabhan et al. (2004) who used models of elliptical galaxies in NFW haloes to argue that

$$V_{\text{circ}}(R_e) = 1.65\sigma_e, \quad (29)$$

with a  $\sim 10\%$  uncertainty in the conversion factor depending on the anisotropy profile. Using similar arguments Schulz et al. (2010) adopt

$$V_{\text{circ}}(R_e) = 1.7\sigma(< R_e). \quad (30)$$

Wolf et al. (2010) argue that  $M_{1/2} \simeq 3\sigma_{\text{los}}^2 r_{1/2}/G$ , where  $M_{1/2}$  is the spherical mass enclosed within the 3D half-light radius,  $r_{1/2}$ , and  $\sigma_{\text{los}}$  is the line of sight velocity dispersion of the whole system. This is equivalent to

$$V_{\text{circ}}(r_{1/2}) = 1.73\sigma_{\text{los}}. \quad (31)$$

For most galaxy light profiles  $r_{1/2} = 1.33R_e$  (Wolf et al. 2010), and since the circular velocity profiles of galaxies typically are close to constant, we expect that  $V_{\text{circ}}(r_{1/2}) \simeq V_{\text{circ}}(R_e)$  to within a few percent. Since the integrated velocity dispersion is expected to be slightly lower than the velocity dispersion within the projected half-light radius. Eqs. 29-31 are expected to be roughly equivalent.

Using Schwarzschild models of 25 early-type galaxies and the assumption of a mass follows light model, Cappellari et al. (2006) find that the dynamical mass is given by

$$M_{\text{dyn}} = 5.0(\pm 0.1)R_e\sigma_e^2/G. \quad (32)$$

We note that the dynamical mass so defined only makes physical sense if the system has a finite mass (which is the case for a mass follows light model of a galaxy). In all other cases, the radius at which the dynamical mass is measured needs to be specified. The mass follows light assumption is obviously incorrect for galaxies embedded in dark matter haloes, but if the baryons dominate within the optical part of the galaxy (for example the half light radius), then mass follows light models may be a reasonable approximation. Models with a dark matter halo typically have flatter velocity dispersion profiles than those without (e.g., Fig. 5 in Cappellari et al. 2006). Thus when one fits a galaxy which contains stars and a dark halo using a model with just stars, the model will tend to overestimate the total mass at small radii and underestimate it at large radii. Since the SAURON kinematics used by Cappellari et al. (2006) are typically confined to less than  $R_e$ , we expect that their mass follows light models underestimate the total mass within  $R_e$ .

The conventional way of writing the dynamical mass (Eq. 32), can be reinterpreted in terms of a more dynamically meaningful mass, namely the mass enclosed within the half light radius. The half-light radius contains half the projected light, by definition. But for a Hernquist sphere (which approximates a de Vaucouleurs profile in projection) the half-light radius encloses (in 3D space) 41.6% of the light. The mass follows light assumption means that

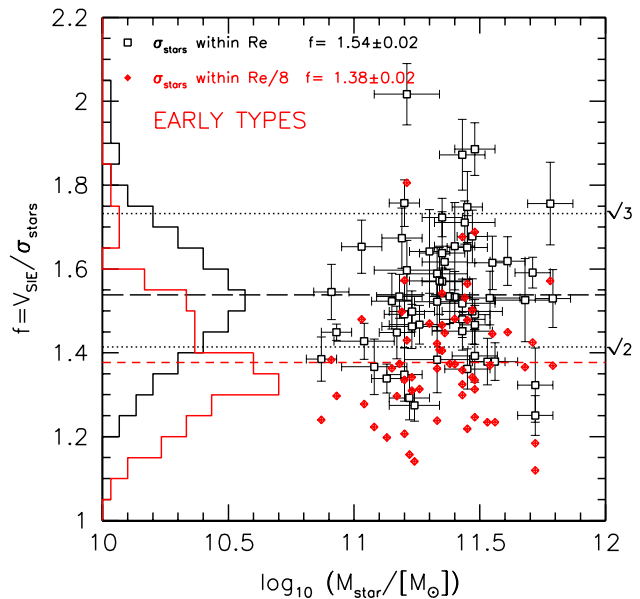


**Figure 8.** Relation between circular velocity from strong gravitational lensing to stellar velocity dispersion. The black squares show the ratio with velocity dispersion measured within the (rest-frame V-band) effective radius,  $R_e$ , while the red diamonds show the ratio with velocity dispersion measured within  $R_e/8$ . For velocity dispersion measured within  $R_e$  the median conversion factor between velocity dispersion and circular velocity is  $f = 1.54$ .

$M_{\text{dyn}} = M_{\text{star}}$ , and thus the 3D mass within the 2D half-light radius is given by

$$M(< R_e) = 0.416M_{\text{dyn}} = 2.08(\pm 0.04)R_e\sigma_e^2/G. \quad (33)$$

Writing this in terms of circular velocities gives

$$V_{\text{circ}}(R_e) = 1.44(\pm 0.01)\sigma_e. \quad (34)$$

We thus see that the dynamical masses derived by Cappellari et al. (2006) are inconsistent with those derived by Padmanabhan et al. (2004), Schulz et al. (2010), and Wolf et al. (2010). In particular, the dynamical masses used by Schulz et al. (2010) are a factor of 1.39 times higher than those of Cappellari et al. (2006). This difference helps to explain why the dark matter fractions are so much higher ( $\sim 60\%$ ) for galaxies in Schulz et al. (2010) than in Cappellari et al. (2006) ( $\sim 30\%$ ), even though the IMFs are nominally the same.

Strong gravitational lensing gives robust measurements (typical accuracy of  $\sim 1\%$ ) of the total projected mass within the Einstein radius. Using lenses from the SLACS survey (Bolton et al. 2006, 2008a), Bolton et al. (2008b) find that the velocity dispersion of the singular isothermal ellipsoid (SIE) lens model,  $\sigma_{\text{SIE}}$ , is similar to the velocity dispersion of the stars. When using the SDSS fiber velocity dispersions they find  $\sigma_{\text{fiber}} = 0.948 \pm 0.008\sigma_{\text{SIE}}$ , and after correcting velocity dispersions to  $R_e/8$  using the empirical formula of Jorgensen et al. (1995), they find  $\sigma(R_e/8) \equiv \sigma_{e8} = 1.019 \pm 0.008\sigma_{\text{SIE}}$ . Converting lens velocity dispersions into circular velocities using  $V_{\text{SIE}} = \sqrt{2}\sigma_{\text{SIE}}$  results in

$$V_{\text{SIE}} = 1.39(\pm 0.01)\sigma_{e8}. \quad (35)$$

This motivates a conversion factor of  $\simeq \sqrt{2}$  between central

velocity dispersion and circular velocity. However, since the velocity dispersion decreases with increasing radius, measuring the velocity dispersion within a larger aperture will result in a larger conversion factor between dispersion and circular velocity. Furthermore, since the typical Einstein radii of SLACS lenses is  $\simeq 0.5R_e$ , the lensing data more closely constrain the circular velocity at radii significantly greater than  $R_e/8$ .

In Fig. 8 we show results using data from SLACS survey as presented in Auger et al. (2009, 2010b). The median stellar mass is  $2 \times 10^{11} M_\odot$ , with a range of  $\sim 1 - 4 \times 10^{11}$  (assuming a Chabrier IMF). We correct the SDSS fiber (3 arcsec diameter) velocity dispersions into dispersions within  $R_e$  and  $R_e/8$  using the quadratic formula<sup>4</sup> from Jorgensen et al. (1995). We find

$$V_{\text{SIE}}/\sigma_{e8} = 1.38 \pm 0.02, \quad (36)$$

and

$$V_{\text{SIE}}/\sigma_e = 1.54 \pm 0.02, \quad (37)$$

where the errors are the statistical uncertainty. The main systematic uncertainty is from the conversion of fiber velocity dispersions to other apertures. For  $\sigma_e$  the mean correction is -0.01 dex, and thus the uncertainty on the correction can be ignored. For  $\sigma_{e8}$  the mean correction is 0.038 dex, and thus the systematic uncertainty might be comparable or larger to the statistical uncertainty.

To summarize, the strong gravitational lensing masses favor a conversion factor between velocity dispersion within the effective radius and circular velocity at the effective radius,  $f = V_{\text{circ}}(R_e)/\sigma(< R_e)$ , roughly half way between  $\sqrt{2}$  and  $\sqrt{3}$ . The dynamical modeling from Cappellari et al. (2006) results in a slightly lower conversion factor, but we expect that this is underestimated due to the assumption that mass follows light.

In what follows we will adopt a conversion factor of  $f = 1.54^{+0.11}_{-0.10}$ , i.e., the uncertainty on  $f$  is 0.03 dex. This uncertainty encompasses the conversion factors of 1.44 from Cappellari et al. (2006) and 1.65 from Padmanabhan et al. (2004).

### 3.8 Gas mass - stellar mass relation

Late-type galaxies generally have gas fractions that increase with decreasing stellar mass or luminosity (e.g., McGaugh & de Blok 1997; Kannappan 2004, Geha et al. 2006, Baldry et al. 2008, Catinella et al. 2010). Fig. 9 shows the relation between gas-to-stellar mass ratio and stellar mass for late-type galaxies using data from Swaters (1999), Verheijen (2001), Garnett (2002), Geha et al. (2006), Leroy et al. (2008) and Catinella et al. (2010). A factor of 1.36 correction for helium has been included in all gas masses either by us or the original authors. The stellar masses have been measured using relations between color ( $B-V$  or  $B-R$ ) and  $M/L$  from Bell et al. (2003), with 0.1 dex subtracted, and then converted to MPA/JHU masses using Eq. 20. All data sets include atomic hydrogen, Garnett (2002) and Leroy et al. (2008) also include molecular hydrogen. For stellar

<sup>4</sup> Using the quadratic formula results in a correction of  $\sigma_{e8}/\sigma_e = 1.117$ , compared to  $\sigma_{e8}/\sigma_e = 1.087$  from the linear formula.

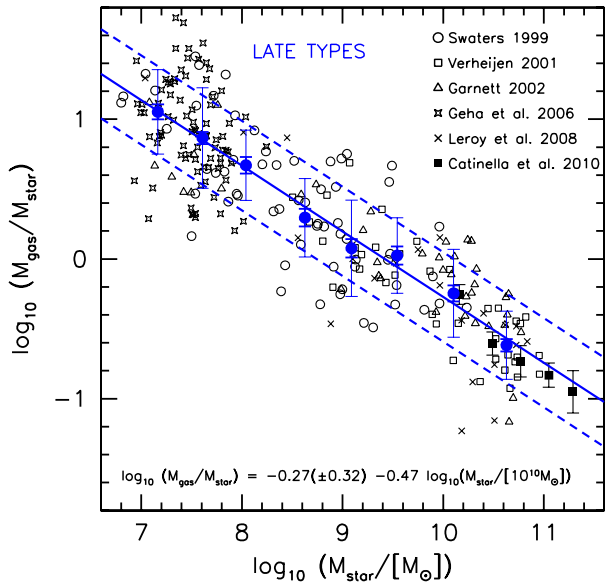


**Figure 9.** Gas-to-stellar mass ratio vs stellar mass for late-type galaxies. The gas is the cold atomic and molecular gas, including Helium. The relation is well fit with a power-law as given, with a scatter of 0.32 dex, which is independent of stellar mass.

masses above  $10^{10} M_\odot$  the mean ratio between molecular hydrogen and stellar mass is 8%. For the samples without molecular gas we apply this factor to derive the mean molecular gas mass. Theoretical support for this conversion comes from semi-analytic models (Dutton, van den Bosch, & Dekel 2010a), which find that the ratio between molecular gas and stellar mass at redshift  $z = 0$  is  $\simeq 8\%$ , independent of stellar mass, and with small scatter  $\simeq 0.1$  dex.

The gas mass - stellar mass relation in Fig. 9 is well fitted by

$$\log_{10} \left( \frac{M_{\text{gas}}}{M_{\text{star}}} \right) = -0.27 - 0.47 \log_{10} \left( \frac{M_{\text{star}}}{10^{10} M_\odot} \right). \quad (38)$$

As specific examples, for a stellar mass of  $M_{\text{star}} = 10^{11} M_\odot$ , the mean gas fraction is 15% (which is divided roughly equally between atomic and molecular gas), while for a stellar mass  $M_{\text{star}} = 10^9 M_\odot$ , the cold gas fraction is 61% (which is dominated by atomic gas). The observed scatter in gas-to-stars ratio is a factor of  $\simeq 2$ , and is independent of stellar mass.

The majority of galaxies with non-detections in the massive galaxy sample ( $M_{\text{star}} > 10^{10} M_\odot$ ) of Catinella et al. (2010), and the dwarf galaxy sample ( $M_{\text{star}} \sim 10^8 M_\odot$ ) of Geha et al. (2006) are on the red sequence. We thus assume that early-type galaxies have, in general, insignificant amounts of gas to be dynamically important.

### 3.9 Gas size - optical size relation

It is well known that the sizes of atomic gas disks are, on average, larger than the sizes of the stellar disks (e.g., Swaters 1999; Verheijen 2001). Fig. 10 shows the ratio between the disk scale lengths of the atomic HI gas and the  $R$ -band light, for late-type galaxies from the samples of Swaters (1999) and

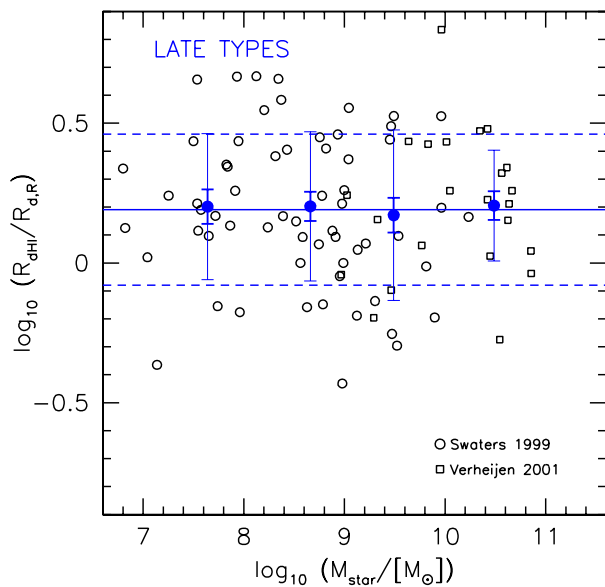


**Figure 10.** Ratio between HI ( $R_{d,HI}$ ) and  $R$ -band ( $R_{d,R}$ ) disk scale lengths vs stellar mass for late-type galaxies, using data from Swaters (1999) and Verheijen (2001). The blue points with error bars show the mean and error on the mean in 4 stellar mass bins of width 1 dex. The mean ratio between HI and  $R$ -band disk scale lengths is independent of stellar mass and is  $\log_{10} R_{d,HI}/R_{d,R} = 0.19 \pm 0.03$ , with a scatter of 0.26 dex.

Verheijen (2001). For the Swaters (1999) sample we use the scale lengths determined by the author. For the Verheijen (2001) sample we use disk scale lengths from McDonald, Courteau, & Tully (2009), and HI disk scale lengths measured by us. In both cases the HI scale lengths are determined from marked fits. That is, the exponential part of the HI density profile is marked by hand, and an exponential profile is fitted to this region. We note that these HI scale lengths are typically measured from the outer part of the HI density profile. The inner part is often constant density or contains a hole. Molecular gas typically dominates over atomic gas in these regions, so that the total gas profile is approximately exponential.

These data span three orders of magnitude in stellar masses, but show no evidence for a mass dependence to the size ratios of atomic and stellar disks. The ratio between the scale lengths of the atomic gas disk and the  $R$ -band light is approximately log-normally distributed, with a mean

$$\log_{10}(R_{d,HI}/R_{d,R}) = 0.19 \pm 0.03 \quad (39)$$

and observed scatter of 0.26 dex. A larger scale length of the atomic gas disk compared to the stellar disk is a natural outcome of a density dependent star formation law (Dutton 2009).

### 3.10 Halo mass - stellar mass relation

We use the relations between the dark matter halo mass,  $M_{200}$ , and stellar mass for central early-type and late-type galaxies from Dutton et al. (2010b). The virial radius of the dark matter haloes are defined such that the mean density

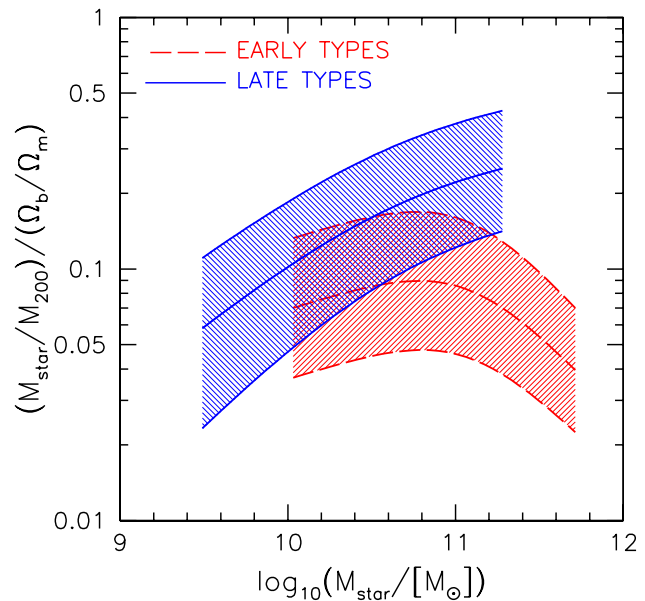


**Figure 11.** Halo mass vs Stellar mass relation for early-types (red) and late-types (blue) expressed in terms of the integrated star formation efficiency, assuming a Chabrier (2003) IMF. The shaded regions correspond to the systematic uncertainty in halo masses at fixed stellar mass. For early-type galaxies of all masses and most late-type galaxies the integrated star formation efficiency is less than 20%.

of the halo is 200 times the critical density of the universe. The halo mass is calculated as the log of the mean halo mass at fixed stellar mass:  $\log_{10} \langle M_{200} \rangle (M_{star})$ . Dutton et al. (2010b) combines halo masses measured from satellite kinematics (Conroy et al. 2007; More et al. 2011), weak lensing (Mandelbaum et al. 2006; Schulz et al. 2010), group catalogs (Yang et al. 2009) and halo abundance matching (Moster et al. 2010; Guo et al. 2010; Behroozi et al. 2010), finding generally good agreement between the different techniques. The results from Dutton et al. (2010b) are shown in Fig. 11, where we have converted the Bell et al. (2003) masses to the MPA/JHU masses using Eq. 20. The shaded regions show the systematic uncertainty in mean halo mass at fixed stellar mass, which is  $\sim 0.25$  dex ( $2\sigma$ ) for both early-types and late-types.

### 3.11 Halo mass - halo concentration relation

Dark matter only simulations in  $\Lambda$ CDM cosmologies have shown there is a tight correlation between halo concentration and halo mass (Navarro, Frenk, & White 1997; Bullock et al. 2001). We adopt the concentration - mass relation for relaxed haloes in a WMAP 5th year cosmology (Dunkley et al. 2009) from Macciò et al. (2008):

$$\log_{10} c_{200} = 0.830 - 0.098 \log_{10} \left( \frac{M_{200}}{10^{12} h^{-1} M_{\odot}} \right). \quad (40)$$

The scatter in this relation for relaxed haloes is  $\simeq 0.11$  dex (Jing 2000; Wechsler et al. 2002; Macciò et al. 2007, 2008). The concentration is correlated with the formation

history of the halo (Wechsler et al. 2002), with earlier forming haloes having higher concentrations.

In this paper we are constructing mass models for the average early-type and late-type galaxy of a given stellar mass. At low masses late-types dominate, so they must form in typical haloes, likewise for high mass early-types. However, low mass early-types, and high mass late-types are minorities, and thus it is plausible that they could form in a biased subset of haloes, and thus their concentrations may be different than the mean. We refer to this bias as a formation bias. The magnitude of the formation bias is constrained by the relatively small scatter in the concentration mass relation.

An additional consideration is that Eq. 40 is for central haloes. Sub-haloes have higher mean concentrations (e.g., Bullock et al. 2001), due to their higher formation redshifts. In the simulation from Klypin et al. (2010) sub-haloes of masses between  $M_{\text{vir}} = 10^{11}$  and  $10^{12}M_{\odot}$  have  $\sim 30\%$  higher concentrations than parent haloes of the same mass. This provides an upper limit to the increase in halo concentrations. However, at fixed stellar mass, sub-haloes are likely to have lower halo masses than parent haloes (Neistein et al. 2011). This counteracts the effect of higher concentrations in sub-haloes, and thus reduces the likelihood that we are underestimating the effective concentrations of low mass dark matter haloes.

Observations show that the satellite fraction is a strong function of stellar mass, with lower satellite fractions at higher stellar masses (Yang et al. 2008). For late-type galaxies the satellite fractions are only  $\sim 30\%$  for stellar masses of  $\sim 10^9M_{\odot}$  and drops to below  $\sim 10\%$  for stellar masses of  $\sim 10^{11}M_{\odot}$ . Thus we do not expect satellite galaxies to bias our results for late-types. At a given stellar mass, the satellite fraction is higher for early-type galaxies than late-type galaxies. For stellar masses of  $\sim 10^{10}M_{\odot}$  the satellite fraction for early-types is  $\sim 50\%$ . Thus it is possible that we are underestimating the concentrations for low mass early-type galaxies by up to  $\sim 30\%$ .

### 3.12 Overview of model parameters and constraints

Our mass model has 9 parameters: 3 for the dark matter halo (mass  $M_{200}$ , concentration  $c$ , and halo contraction model); and 6 for the baryons (stellar mass,  $M_{\text{star}}$ , bulge fraction,  $f_b$ , bulge size,  $R_b$ , stellar disk size,  $R_d$ , cold gas mass,  $M_{\text{gas}}$ , gas disk size,  $R_g$ ). To construct a model galaxy we then apply the following procedure:

- (i) Pick the type of galaxy (i.e., early or late).
- (ii) Pick a stellar mass,  $M_{\text{star}}$ , assuming a Chabrier IMF.
- (iii) The six parameters for the baryons are then specified by the observational constraints (§3.3-3.9), up to the normalization of the stellar mass to light ratio, which we term  $\Delta_{\text{IMF}}$  to suggest this uncertainty is due to the unknown stellar IMF, although it also includes systematic uncertainties in measuring stellar masses for a given IMF.
- (iv) Determine the halo mass from the halo mass - stellar mass relation from Dutton et al. (2010b) as discussed in §3.10, and shown in Fig. 11.
- (v) Determine the halo concentration using Eq. 40 as discussed in §3.11.

Thus our nine model parameters can be reduced to 2 primary unknowns: the stellar IMF normalization, and the halo contraction model. We have one additional constraint, which is the model has to reproduce the observed TF or FJ relation Eqs. 24 & 27. We construct model TF/FJ relations by computing the model at a range of stellar masses. Thus by comparing the observed and model TF/FJ relations for a given IMF we can solve for the halo contraction model. Alternatively, we can assume a halo contraction model and solve for the stellar IMF. Since the model is under constrained, we expect there to be a degeneracy between the IMF and the halo contraction model.

### 3.13 Dark matter fractions

Before we compare our bulge-disk-halo models to the observed TF and FJ relations, some useful insight into the dark matter content of galaxies can be obtained by comparing the baryonic mass within a sphere of some fiducial radius (2.2 disk scale lengths for late-types, the half light radius for early-types) with the spherical mass derived from the optical circular velocity. The baryonic masses within the fiducial radii,  $M_{\text{bar}}(< r)$  are determined using the mass models as described in § 2, with the observational constraints discussed earlier in this section. The total masses within the fiducial radii are determined assuming spherical symmetry, i.e.,  $M_{\text{tot}}(< r) = rV_{\text{circ}}^2(r)/G$ . Thus the baryon fraction is given by  $f_{\text{bar}}(< r) = [V_{\text{bar}}(< r)/V_{\text{tot}}(< r)]^2$ , and the dark matter fraction is given by  $f_{\text{DM}}(< r) = 1 - f_{\text{bar}}(< r)$ . Note that for galaxies with a dominant disk component the assumption of spherical symmetry will cause the total mass to be over-estimated slightly.

The results of this calculation is shown in Fig. 12. For early-type galaxies (left panel) the dark matter fraction is lowest in galaxies with stellar mass  $\sim 10^{10}M_{\odot}$ , and increases for higher and lower mass galaxies. The trend of increasing dark matter fractions in higher mass (or luminosity) early-type galaxies, for a universal IMF, is well established (e.g., Padmanabhan et al. 2004; Gallazzi et al. 2006; Tortora et al. 2009; Auger et al. 2010b, Napolitano et al. 2010). The breaking of this trend at lower masses should not be considered a surprise as dwarf spheroidal galaxies are known to be dark matter dominated within their half-light radii (e.g., Tollerud et al. 2011).

For early-type galaxies a Salpeter IMF is consistent with the dynamical masses, as long as  $V_{\text{circ}}(R_e)/\sigma(< R_e) \equiv V_c/\sigma_e \gtrsim 1.6$ . As shown in § 3.7 the dynamical models of Cappellari et al. (2006) imply that  $V_c/\sigma_e = 1.44 \pm 0.01$ , which, as noted by these authors, disfavors a universal Salpeter IMF. For late-type galaxies (right panel) the dark matter fraction decreases with increasing stellar mass in agreement with previous studies (e.g., McGaugh 2005; Pizagno et al. 2005; Dutton et al. 2007). In late-type galaxies the contribution of the cold gas (as shown by the green dot-dashed line) is small, and for early-type galaxies we assume that the contribution of the cold gas is negligible.

## 4 RESULTS

We now construct mass models for early-type and late-type galaxies, using various assumptions about the stellar IMF,

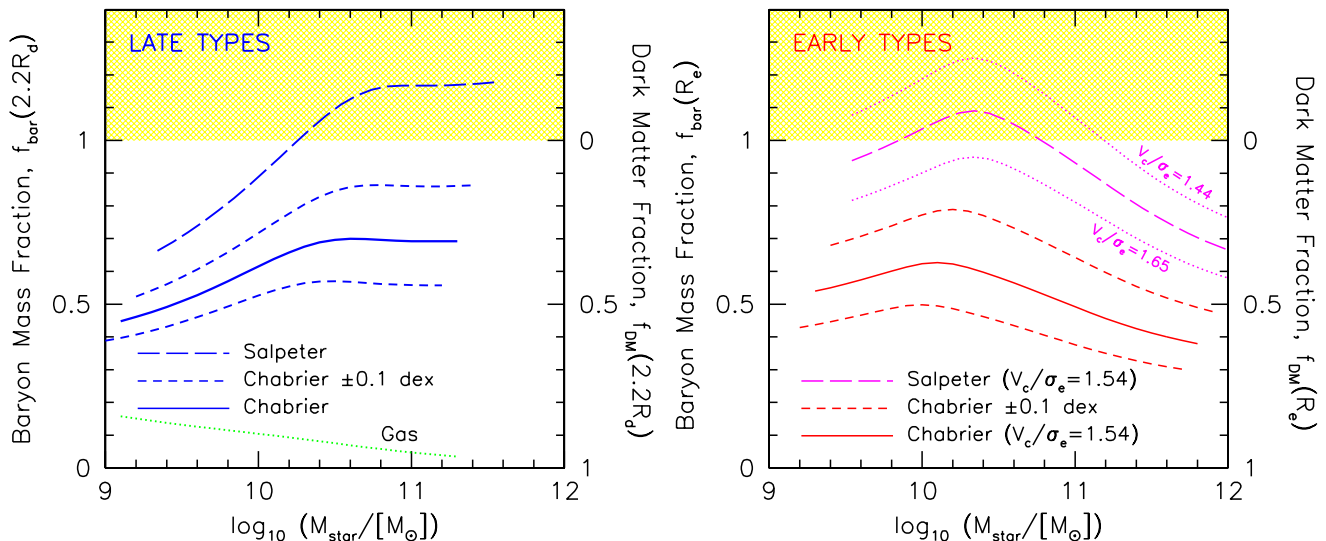


**Figure 12.** Mean baryon mass fractions within the optical part of galaxies as a function of total galaxy stellar mass. For late-types (left panel) the radius is 2.2 stellar disk scale lengths, while for early-types (right panel) it is the projected circularized half-light radius. The solid lines show the results for a Chabrier (2003) IMF. The effect of changing the stellar mass normalization by  $\pm 0.1$  dex is shown by the short-dashed lines, and by  $+0.24$  dex (i.e., a Salpeter IMF) is shown by the long-dashed lines. For late-type galaxies the baryon fractions increase with stellar mass and saturates at  $f_{\text{bar}} \sim 0.7$  at high masses. For early-types the baryon fractions reach a maximum near a stellar mass of  $10^{10} M_{\odot}$ , and declines to higher and lower masses. The yellow shading corresponds to the forbidden region where the baryons over-predict the dynamical mass. A Salpeter IMF over-predicts the dynamical masses for massive late-types, but is allowed for all early-type galaxies unless  $V_c/\sigma_e \lesssim 1.6$ .

and adiabatic contraction, and compare these to the observed optical circular velocity - stellar mass (VM) relations. We start with a model with standard (Gnedin et al. 2004, G04) halo contraction and a standard (Chabrier 2003) IMF. The predicted VM relations for early-type and late-types are shown in Fig. 13. The shaded regions show the systematic uncertainty in the observed relations. The solid lines show the model relations, with the fainter lines corresponding to the systematic uncertainty on the halo masses. Note that for low stellar masses ( $M_{\text{star}} \lesssim 10^{10.0} M_{\odot}$  for early-types and  $M_{\text{star}} \lesssim 10^{9.5}$  for late-types) we have extrapolated the halo mass - stellar mass relation, and thus our results in these regions should be treated with more caution.

The model nicely reproduces the slopes of the VM relations, and the zero point of the VM relation for early-types, but it does not reproduce the zero point for late-types. At fixed stellar mass,  $M_{\text{star}}$ , the optical circular velocity,  $V_{\text{opt}}$ , is over-predicted by the model. This problem is known as the TF zero point problem (e.g., Dutton et al. 2008). As discussed in previous papers (Dutton et al. 2007; Dutton & van den Bosch 2009) there are three principle solutions to this problem of simultaneously matching the rotation velocity - stellar mass (i.e., Tully-Fisher) relation, disk size - stellar mass relation and halo mass - stellar mass relation in the context of  $\Lambda$ CDM.

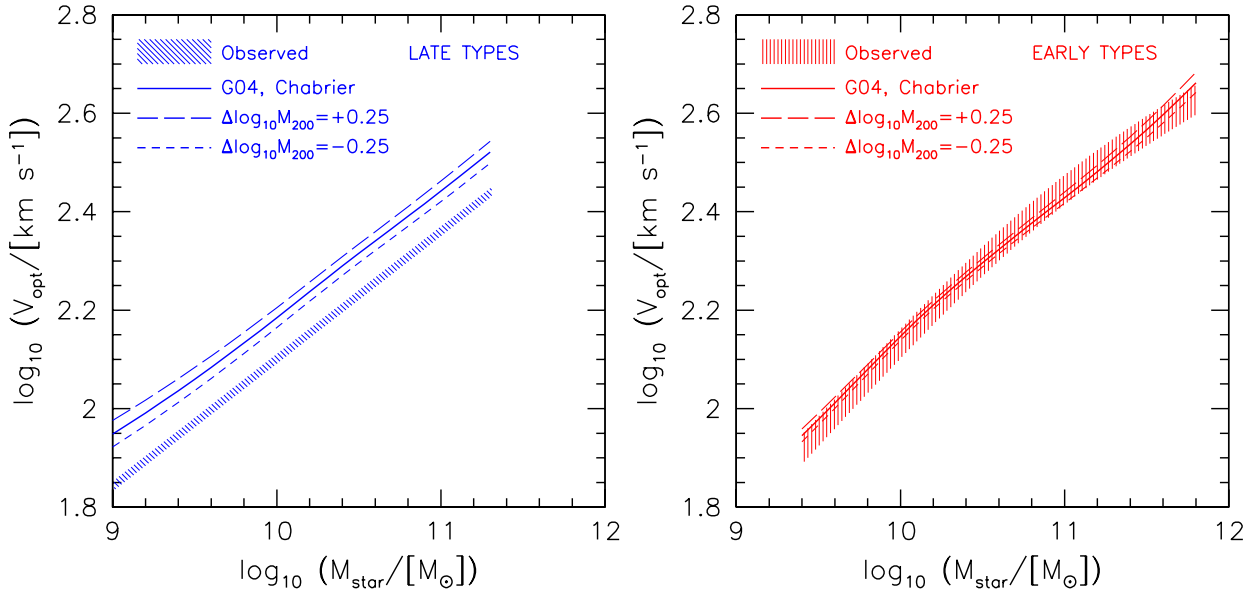
- Reduce the stellar mass.
- Reduce *pristine* halo concentration.
- Reverse or prevent halo contraction.

A change in stellar mass normalization can result from either a systematic error in inferring stellar masses from observed photometry, or due to a change in the stellar IMF. A

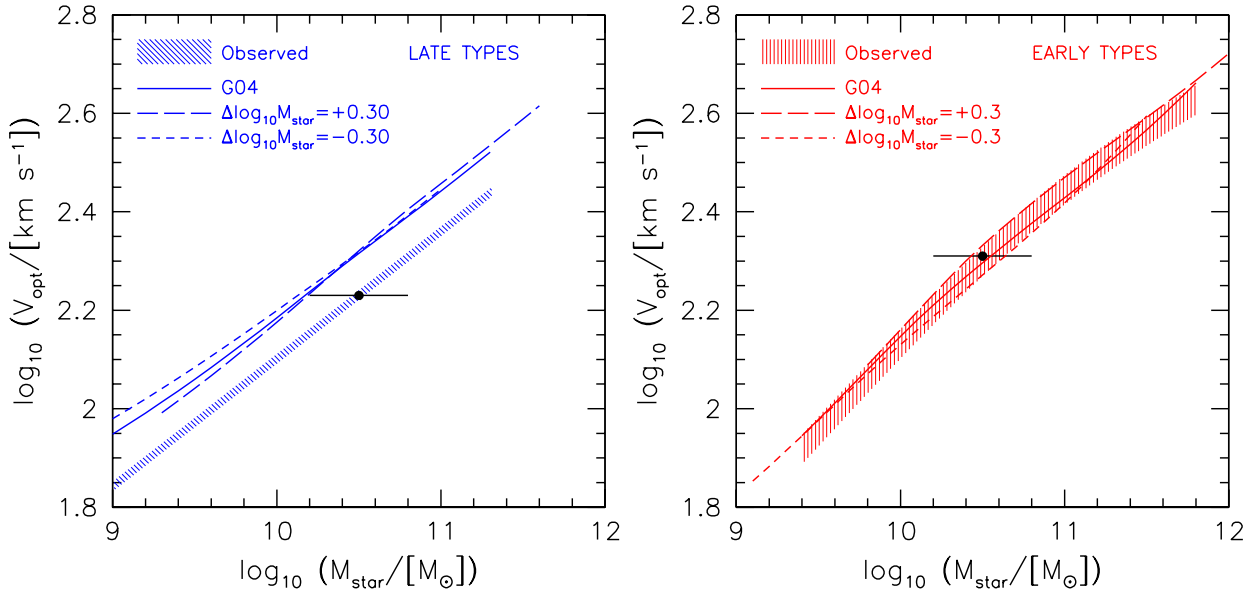
Salpeter IMF results in stellar masses  $\simeq 0.24$  dex higher than a Chabrier (2003) IMF (which we adopt here as our standard IMF). Reducing stellar masses would require an IMF with fewer low mass stars, or conversely, more high mass stars. The latter results in higher luminosities, and hence lower mass-to-light ratios. However, there is a limit to how much the stellar  $M/L$  can be reduced, especially for old or moderately old stellar populations, because stellar populations with bottom light IMFs become dominated by stellar remnants at late times (van Dokkum 2008).

Fig. 14 shows the effects on the VM relation of changing the stellar mass normalization by  $\pm 0.3$  dex. The horizontal bar shows the changes this causes in the observed relation. Interestingly, the model relations are largely unaffected by these changes in stellar mass. This is because increasing the stellar mass (at fixed galaxy size and halo mass) results in higher optical circular velocity, and vice versa for lower stellar masses. Thus changes in the stellar mass normalization move model galaxies along the VM relation. Fig. 14 shows that to reconcile a model with standard halo contraction with the observed VM relation of late-type galaxies requires stellar masses lower by a factor of  $\sim 2$ . However, lowering the stellar masses of early-type galaxies by the same factor would remove the agreement. This suggests that early-type and late-type galaxies cannot share the same IMF and halo response to galaxy formation.

A change in the “*pristine*” halo concentration could be possible by either a formation bias, since halo concentration is strongly correlated with halo formation time (Wechsler et al. 2002), or a change in cosmology. The magnitude of any formation bias is constrained by the scatter in halo concentrations. For relaxed haloes, the scatter in halo con-



**Figure 13.** TF and FJ relations for models with Gnedin et al. (2004, G04) halo contraction and a Chabrier (2003) IMF. The observations, with  $2\sigma$  uncertainties, are given by shaded regions. The dashed lines show the effect on the model by changing the halo masses by  $\pm 0.25$  dex, which corresponds to the  $2\sigma$  systematic uncertainty. The model reproduces the slopes of both relations, and the zero point of the FJ relation, but not the zero point of the TF relation.



**Figure 14.** Effect of stellar mass normalization on  $V_{\text{opt}} - M_{\text{star}}$  relations for early-type (right panel) and late-type (left panel) galaxies. The model relations are approximately independent to changes in stellar mass normalization of  $\pm 0.3$  dex. This is because models with higher stellar masses (at fixed sizes and halo masses) also have higher  $V_{\text{opt}}$ . By contrast the observed relations are strongly dependent on the stellar mass normalization (black horizontal bar). Thus reconciling the standard halo contraction model with observations requires late-type galaxies have stellar masses lower by factor of  $\sim 2$ .

centrations, at fixed halo mass, is  $\simeq 0.11$  dex (e.g., Jing 2000; Wechsler et al. 2002; Macció et al. 2007). At low stellar masses ( $M_{\text{star}} < 10^{10} M_{\odot}$ ) the majority of galaxies are late-types, and thus a formation bias is only expected to effect early-type galaxies. At high stellar masses  $M_{\text{star}} \gtrsim 10^{11} M_{\odot}$ )

the majority of galaxies are early-types, and thus a formation bias is only expected to effect late-types.

An alternative way to reduce the initial halo concentrations is to reduce the amplitude of the power spectrum on galaxy scales. The most effective way to achieve this is through a change in  $\sigma_8$  (the amplitude of the linear power



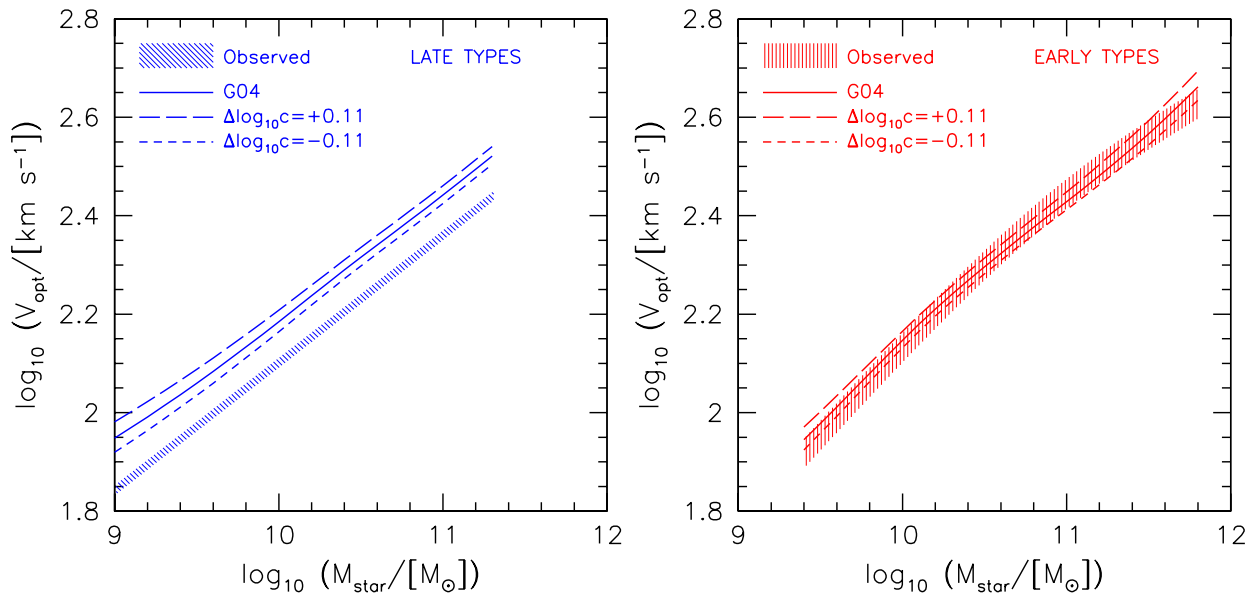


**Figure 15.** Effect of halo concentration on  $V_{\text{opt}} - M_{\text{star}}$  relation for early-type (right panel) and late-type (left panel) galaxies. Higher halo concentrations result in higher optical circular velocities. The scatter in halo concentrations is  $\simeq 0.11$  dex (Macciò et al. 2008), and thus concentrations biases in both early-type and late-type galaxies are likely to be small.

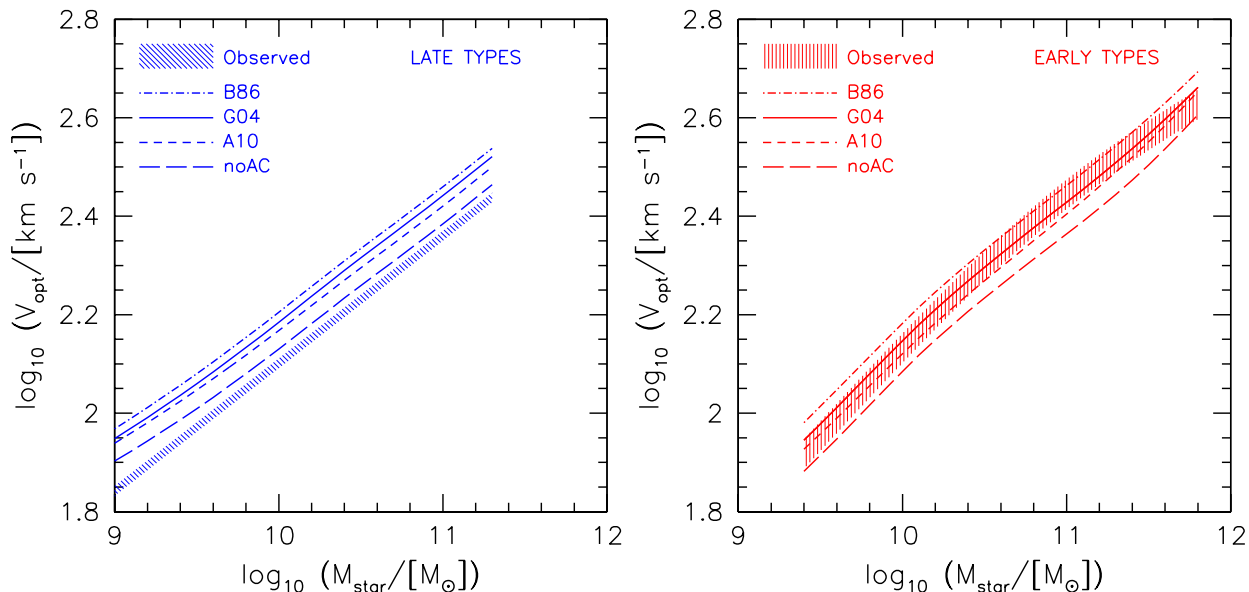


**Figure 16.** Effect of adiabatic contraction on  $V_{\text{opt}} - M_{\text{star}}$  relation for early-type (right panel) and late-type (left panel) galaxies. Adiabatic contraction results in higher optical circular velocities. Compared to a model with no halo contraction (long dashed lines), the increase in optical circular velocities is  $\simeq 0.1$  dex for the Blumenthal et al. (1986, B86) model,  $\simeq 0.08$  dex for the Gnedin et al. (2004, G04) model, and  $\simeq 0.05$  dex for the Abadi et al. (2010) model. For these models (with a Chabrier IMF and standard halo concentrations) early-type galaxies favor models with strong halo contraction, whereas late-type galaxies favor models with halo expansion.

spectrum today on scales of  $8h^{-1}\text{Mpc}$ ). The concentration scales roughly linearly with  $\sigma_8$ , so that a 0.11 dex change in halo concentrations (equivalent to the  $1\sigma$  intrinsic scatter) requires a change in  $\sigma_8$  of a factor of  $\simeq 1.3$ . This is much larger than the reported uncertainties in  $\sigma_8$  of 0.014 dex (Komatsu et al. 2009), and thus the uncertainties in halo

concentrations from uncertainties in cosmological parameters are likely to be small.

Fig. 15 shows the effect of changing the halo concentration (by  $\pm 0.11$  dex, i.e., the  $1\sigma$  intrinsic scatter) on the VM relations of the standard model. Increasing/decreasing the halo concentration results in higher/lower  $V_{\text{opt}}$ . The changes are relatively small. For high mass late-type galaxies a for-

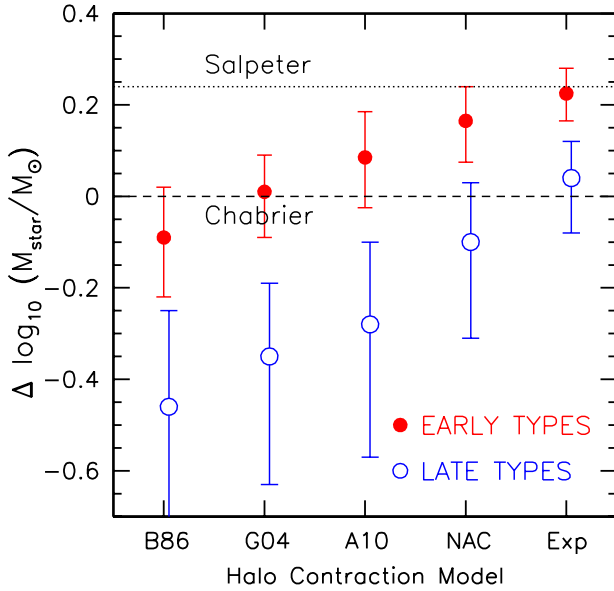


**Figure 17.** Offset in stellar masses required to match the zero point of the VM relations as a function of halo response model, calculated at  $\log_{10}(V_{\text{opt}}/\text{km s}^{-1}) = 2.30$ , for early-type (red filled symbols) and late-type (blue open symbols) galaxies. The models correspond to: B86 (Blumenthal et al. 1986); G04 (Gnedin et al. 2004); A10 (Abadi et al. 2010); NAC no halo contraction; Exp (halo expansion with  $\nu = -0.5$  in Eq. 17). The error bars show the effects of  $2\sigma$  systematic errors on the zero points of the VM and  $M_{200}$ - $M_{\text{star}}$  relations. For fixed IMF (i.e., horizontal lines) early-type galaxies require stronger contraction than late-type galaxies, while for fixed halo response (vertical direction) early-type galaxies require heavier IMFs than late-type galaxies.

mation bias resulting in 0.1 dex lower halo concentrations is the most that is feasible, but this has very little effect on the zero point of the VM relation. Thus changes in halo concentrations are not likely to resolve the TF zero point problem.

As discussed in § 2.2.1, recent cosmological simulations suggest that the Gnedin et al. (2004) halo contraction formalism over-predicts the amount of halo response (Abadi et al. 2010; Tissera et al. 2010; Pedrosa et al. 2010). Fig. 16 shows the effect of the halo contraction model on the VM relations adopting a Chabrier IMF. The differences in  $V_{\text{opt}}$  between a model with no contraction and the Blumenthal et al. (1986, B86) model are  $\simeq 0.1$  dex, for both early-type and late-types. The Gnedin et al. (2004, G04) model results in only slightly less contraction than the B86 model. The Abadi et al. (2010, A10) model results in  $\simeq 0.05$  dex increase in  $V_{\text{opt}}$ , so that the VM relation lies half way between the B86 model and no contraction. The model without halo contraction is only marginally consistent with the observed VM relation for late-types, and thus a model with halo expansion would fit the data better. For early-types the Gnedin et al. (2004) halo contraction model provides the best fit to the data, assuming a Chabrier IMF. The B86 and A10 halo contraction also provide acceptable fits given uncertainties in halo masses.

#### 4.1 Implications for a universal IMF and halo response

We have shown that a model with standard halo contraction and a Chabrier stellar IMF reproduces the slopes of the VM relations of early-type and late-types, and the zero point of the VM relation for early-types, but not the zero point for late-types. Fig. 17 shows the offsets in stellar mass required to match the zero point of the VM relations. Early-types are shown with red filled symbols and late-types with blue open symbols. The error bars correspond to the  $2\sigma$  uncertainty in the observed VM zero point and halo masses. This shows that for any given halo response model, a simultaneous match of the VM relations for early-type and late-types requires different stellar mass normalizations. Alternatively, for models with a universal IMF, early-types require stronger halo contraction than late-types.

More specifically, for models with halo contraction (B86, G04, A10) early-type galaxies require stellar masses higher by a factor of  $\simeq 2$  than late-types. For early-type galaxies halo contraction models are consistent with a Chabrier IMF. For late-types halo contraction models require lighter IMFs than Chabrier (at least 0.1 dex for A10, 0.2 dex for G04 and 0.25 dex for B86). For models with uncontracted NFW haloes early-types favor an IMF  $\simeq 0.17$  dex heavier than Chabrier, while late-types favor an IMF  $\simeq 0.1$  dex lighter than Chabrier.

#### 4.2 Circular velocity profiles and the bulge-disk-halo conspiracy

So far our analysis has considered only the optical circular velocity at a single radius. But there is potentially useful information to be obtained by including circular velocity measurements at additional radii. In addition, the close to constant circular velocity profiles in the optical regions of early and late-type galaxies has often been termed a ‘‘conspiracy’’ between the baryons and the dark matter (e.g., van Albada & Sancisi 1986; Koopmans et al. 2009).

Fig. 18 shows example model circular velocity profiles for early-type and late-type galaxies at a range of stellar masses. These models have stellar masses according to Chabrier IMF and halo response chosen to reproduce the FJ and TF relations. For early-type galaxies this requires Gnedin et al. (2004) halo contraction, while for late-type galaxies this requires halo expansion with  $\nu = -0.5$  in Eq. 17. The axes are scaled to the virial radii and circular velocities. For each galaxy model, the right panel shows the model out to the virial radius,  $R_{200}$ , while the left panel shows the model in the inner 4% of  $R_{200}$  for early-types and the inner 10% of  $R_{200}$  for late-types. To give a common reference point to the scales in the various panels, the dotted vertical lines corresponds to 10 kpc.

It is immediately apparent that these model galaxies have roughly constant circular velocity profiles, especially within a few optical half-light radii. As previously shown in Dutton et al. (2010b) we find that both early-types and late-types have  $V_{\text{opt}}/V_{200} \simeq 1$ , where  $V_{\text{opt}} = V_{2.2}$  for late-types and  $V_{\text{opt}} = V_{\text{circ}}(R_e)$  for early-types. We do note however, that the mass profiles are not exactly isothermal between the optical half-light radius and the virial radius. Outside the inner  $\sim 10\%$  of the virial radius the circular velocity

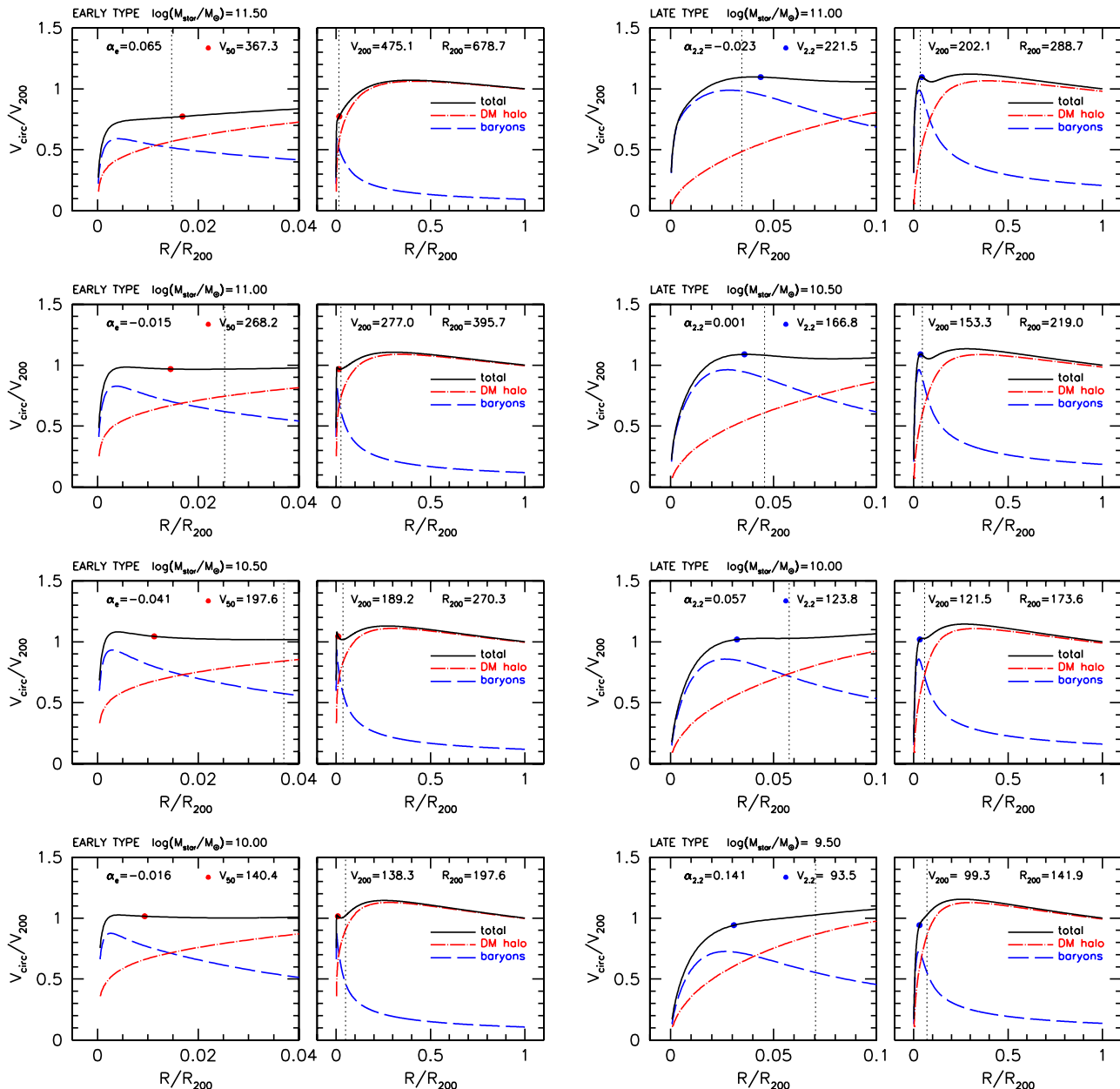


**Figure 18.** Circular velocity profiles for model early-type galaxies (left panels) and late-type galaxies (right panels) that reproduce the FJ and TF relations, respectively. All models have a Chabrier (2003) stellar IMF. The early-type galaxy models have halo contraction according to Gnedin et al. (2004), while the late-type galaxies have halo expansion with  $\nu = -0.5$  in Eq. 17. For each model galaxy the two panels show the circular velocity profiles out to the virial radius, and the inner 4%/10% of the virial radius, or early-type/late-type galaxies. To give a physical reference point, in all panels the vertical dotted line corresponds to 10 kpc. The stellar masses (in  $M_{\odot}$ ), virial circular velocities (in  $\text{km s}^{-1}$ ) and virial radii (in kpc) decrease from top to bottom as indicated. For early-type galaxies the red dot corresponds to the circular velocity at the effective radius, which occurs at  $\sim 1\%$  of the virial radius. The logarithmic slope of the circular velocity profile at the effective radius is given by  $\alpha_e$  and is close to zero for all galaxies. Likewise, for late-type galaxies the blue dot corresponds to the circular velocity at 2.2 optical disk scale lengths radius, which occurs at  $\sim 4\%$  of the virial radius. The logarithmic slope of the circular velocity profile at 2.2 scale lengths is given by  $\alpha_{2.2}$  which is also close to zero for all galaxies.

profiles rise, reaching a maximum at  $\sim 30\%$  of the virial radius.

The shape of the circular velocity profiles can be quantified by the logarithmic slope at a given radius:

$$\alpha(r) = \partial \log V_{\text{circ}}(r) / \partial \log r. \quad (41)$$

For a spherical mass density with  $\rho(r) \propto r^{-\gamma}$ , the slope

of the density profile is related to the slope of the circular velocity profile via  $\gamma = 2 - 2\alpha$ .

By combining strong gravitational lensing with stellar dynamics Koopmans et al. (2009) found that for massive early-type galaxies the mass density slope within the effective radius  $\gamma = 2.085^{+0.025}_{-0.018}$ , assuming isotropic velocity dispersions, with a systematic uncertainty of  $\simeq 0.1$ . Other

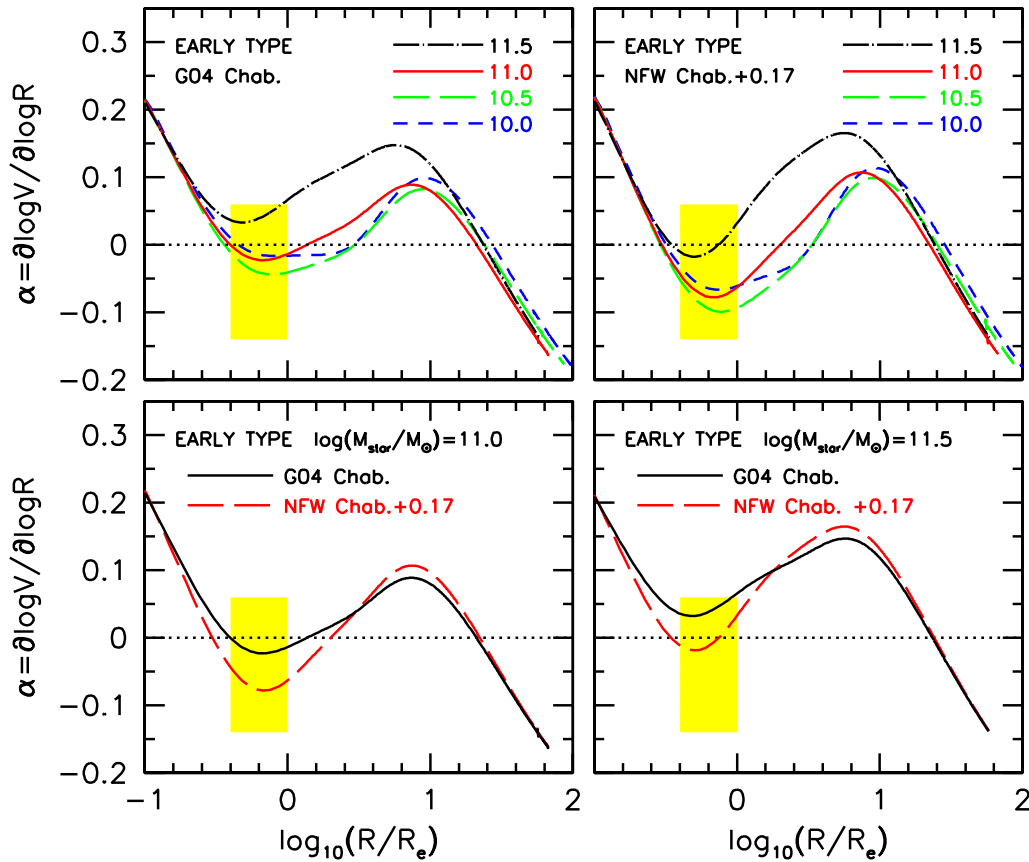


**Figure 19.** Logarithmic slope of the circular velocity profile for early type galaxies. The upper panels show the dependence on stellar mass, with  $\log_{10}(M_{\text{star}}/M_{\odot})$  as indicated (normalized to a Chabrier IMF). The upper left panel shows models with Gnedin et al. (2004; G04) halo contraction and a Chabrier IMF, while the upper right panel shows models with uncontracted NFW haloes and stellar masses 0.17 dex higher than a Chabrier IMF. Both of these models reproduces the FJ relation. All models have close to isothermal ( $\alpha = 0$ ) circular velocity profiles over a wide range of radii, and in particular in the region of overlap between baryonic and dark matter. The yellow shaded region shows the observed value (with  $2\sigma$  systematic uncertainties) for massive [ $11 \lesssim \log_{10}(M_{\text{star}}/M_{\odot}) \lesssim 11.6$ ] early type galaxies from Koopmans et al. (2009). Both sets of models are consistent with these data. The lower panels show the difference between models with and without halo contraction for  $\log_{10}(M_{\text{star}}/M_{\odot}) = 11.0$  (lower left) and  $\log_{10}(M_{\text{star}}/M_{\odot}) = 11.5$  (lower right). Distinguishing between these models requires measuring  $\alpha$  to better than 5%.

authors find similar mean values of  $\gamma$  (e.g., Dobke & King 2006; Auger et al. 2010; Barnabe et al. 2011). Thus the results from Koopmans et al. (2009) are consistent with  $1.88 \lesssim \gamma \lesssim 2.29$  (at the  $2\sigma$  level), which corresponds to  $-0.14 \lesssim \alpha \lesssim 0.06$ . Our models for massive early-types are within this range and thus are consistent with current observational constraints (Fig. 19).

Models with different halo response and IMFs can give different values of  $\alpha$ . For example, an early-type galaxy with a stellar mass of  $M_{\text{star}} = 10^{11} M_{\odot}$  assuming a Chabrier IMF and Blumenthal et al. (1986) halo contraction results in  $\alpha(R_e) \simeq -0.01$ , while a model with 0.17 dex higher stellar mass and no halo contraction results in  $\alpha(R_e) \simeq -0.06$ . Both of these models reproduce the observed circular velocity at  $R_e$ , but the model without halo contraction has higher circular velocities at smaller radii because of the more massive baryonic component. So in principle, measuring the slope of the total mass profile within the effective radius can help to discriminate between models with different halo response and IMF. However, the current systematic uncertainties in

$\alpha$  are  $\sim 0.05$ , which is similar to the differences we wish to measure.

The fact that  $\alpha \simeq 0$  is sometimes referred to as the bulge-halo *conspiracy* for early-types and disk-halo *conspiracy* for late-types (e.g., van Albada & Sancisi 1986; Koopmans et al. 2009). A conspiracy implies that there is an underlying physical mechanism that forces galaxies to have  $\alpha \simeq 0$ , despite numerous ways in which galaxies would otherwise have  $\alpha \neq 0$ . Sometimes halo contraction is invoked as such a mechanism (e.g., Blumenthal et al. 1986; Klypin et al. 2002). However, we find that models with different halo responses (contraction, no contraction and expansion) and different IMFs all result in  $-0.2 \lesssim \alpha \lesssim 0.2$  for a wide range of galacto-centric radii  $0.1 \lesssim R/R_e \lesssim 100$ . Thus the observations fact that  $\alpha \simeq 0$  cannot be used to discriminate between different models for halo response. Rather, our results suggest that  $\alpha \simeq 0$ , over a wide range of radii, is a natural consequence for galaxies embedded in  $\Lambda$ CDM haloes.

Using cosmological hydrodynamical simulations Duffy

et al. (2010) find a tension between the need for strong feedback (in order to reproduce the observed low baryon fractions) and the need for strong dissipation (in order to match the isothermal density profiles inferred from lensing/dynamics). This is in conflict with our results which show that early-type galaxies embedded in  $\Lambda$ CDM haloes with the correct baryon fractions reproduce isothermal density profiles within an effective radius. Thus we do not support the idea that the lensing observations are biased towards galaxies with steeper density profiles. Rather, the tension found by Duffy et al. (2010) may simply be the result of systematic effects in the comparison between simulations and observations. The main cause for concern is that the simulated galaxies are at  $z = 2$  whereas the observed galaxies are at  $z \sim 0$ . This makes it hard to know the appropriate radii within which to measure  $\gamma$ . Since  $\gamma$  depends on radius, it is critical to compare observations and simulations at the same radii.

## 5 DISCUSSION

We have established that either the stellar initial mass function, or the halo response to galaxy formation cannot be the same for early-type galaxies (ETGs) and late-type galaxies (LTGs). We now discuss physical mechanisms that could cause halo response to be different from the standard adiabatic contraction hypothesis, and others which could cause the IMF to vary. We discuss how these mechanisms might vary with galaxy type, and hence if they can explain, qualitatively our results.

Two defining differences between ETGs and LTGs that may have consequences of the IMF and halo response, are the concentration of the stars and the star formation histories. ETGs have higher concentrations (associated with a spheroidal component) and they formed the bulk of stars at earlier times than LTGs.

### 5.1 What could cause halo contraction to vary with galaxy type?

There are a number of processes that occur during galaxy formation which can alter the structure of the dark matter halo. Some of these can also alter the morphological type of a galaxy. We outline these processes below.

- **Smooth accretion:** Smooth accretion of gas onto the central galaxy is the quintessential process that is expected to result in (adiabatic) halo contraction (Blumenthal et al. 1986). This process is expected to result in disk growth and star formation, and thus LTGs, but it could also occur during the history of ETGs.

- **Dissipative major mergers:** Major mergers which involve significant amounts of gas a.k.a. “wet mergers” are expected to result in halo contraction due to the mass that accumulates at the center of the galaxy. This process turns LTGs into ETGs.

- **Non-dissipative major mergers:** Major mergers which do not involve gas a.k.a. “dry mergers” are expected to result in effective halo contraction due to mixing of stars and dark matter through violent relaxation. This contraction effect partially undoes the segregation of baryons and dark matter

produced by dissipation. Note that this is a different physical process than the standard adiabatic halo contraction. This process only occurs for ETGs.

- **Clumpy accretion/minor mergers:** Clumpy accretion of stars or gas in the form of minor mergers can cause halo expansion due to dynamical friction (e.g., El-Zant et al. 2001, Elmegreen et al. 2008; Romano-Diaz et al. 2008; Johansson et al. 2009). The clumps need to be baryon dominated, or else dark matter will be brought in to replace the dark matter that is removed by dynamical friction. The clumps also need to be dense, or else they will be tidally disrupted before they can alter the center of the halo. Clumpy cold accretion is more likely to occur at high redshifts (Dekel et al. 2009). This process can occur in both ETGs and LTGs.

- **Feedback:** The energy and momentum feedback from supernova, stellar winds and AGN can cause halo expansion under the following conditions: (1) By removing large amounts of baryons on a timescale much faster than in which they were accumulated (e.g., Navarro et al. 1996b; Gnedin & Zhao 2002; Read & Gilmore 2005; Governato et al. 2010); or (2) By inducing large scale bulk motions (Mashchenko et al. 2006; 2008). These processes are expected to be more effective in galaxies with the following properties: (1) lower mass and lower bulge fraction (i.e., LTGs), due to the shallower potential wells; (2) higher gas fractions, because a large fraction of the baryons need to be expelled for this process to be effective, and stellar mass cannot be expelled by feedback; (3) higher redshifts, due the order of magnitude higher specific star formation rates.

- **Bars:** Galactic bars can cause halo expansion due to dynamical friction on the bar from the dark matter halo (Weinberg & Katz 2002). Since gas can get driven to the center of the galaxy, bar formation could also result in halo contraction. Bars require disks in which to form, and since bulges help to stabilize disks, bars are more frequent in late-type galaxies. However, bars are known to exist in S0 galaxies, which are considered to be ETGs, and thus the effects of bars on dark matter haloes are not necessarily restricted to LTGs.

Major mergers have long been thought to be the key process that determines the morphological type of a galaxy (Toomre & Toomre 1972), with major mergers destroying disks, and producing spheroidal galaxies. Galaxy types are observed to vary strongly with stellar mass: low mass galaxies are predominately late-types (disk dominated, gas rich, star forming), while high mass galaxies are predominantly early-types (bulge dominated, gas poor, non star forming). This basic trend can be understood as a consequence of the mass dependence of the frequency of major mergers and the mass dependence of gas fractions of the progenitor galaxies (Maller 2008; Hopkins et al. 2009a,b). The mass dependence of the effects of dissipative major mergers can also qualitatively explain the tilt of the Fundamental Plane (Dekel & Cox 2006).

Thus the key physical process that occurs during early-type galaxy formation, which does not occur during late-type galaxy formation, is a major merger. Whether the merger is dissipative or non-dissipative we expect the haloes to contract, but for different reasons. This expectation needs to be tested, and quantified, with numerical simulations of galaxy/halo mergers. For late-type galaxies, a combination

of clumpy cold accretion, and feedback during the early phases of galaxy formation could plausibly result in net halo expansion (e.g., Mo & Mao 2004).

Under this scenario, galaxies with a higher fraction of their stars in a spheroid (i.e., a classical bulge) should have experienced more halo contraction. This is qualitatively consistent with our result that for a fixed IMF early-type galaxies have more halo contraction than late-type galaxies (e.g., Fig. 17). To test this further for early-types and late-types separately, would require the velocity - stellar mass, halo mass - stellar mass, and structural scaling relations to be measured for galaxies with different bulge fractions. In the meantime we note that earlier type spirals have higher rotation velocities at fixed K-band luminosity and stellar mass than spiral galaxies in general (Noordermeer & Verheijen 2007; Williams et al. 2010). Such a trend would be expected if earlier type spirals experienced more halo contraction than later type spirals. But there could be other explanations, such as more compact baryons, so it is too early to say if this supports our simple scenario.

## 5.2 What could cause the IMF to vary with galaxy type?

Observations in the Galactic disk suggest that the IMF has a power-law shape at masses above  $1M_{\odot}$ , and that it turns over at lower masses (Kroupa 2001; Chabrier 2003). This turnover can be modeled by a log-normal distribution with a characteristic turnover mass  $m_c$  (Chabrier 2003). The value of  $m_c$  is  $\sim 0.1M_{\odot}$  in the disk of the Milky Way.

Larson (1998, 2005) has argued that the characteristic turnover mass may largely be determined by the thermal Jeans mass, which strongly depends on the temperature of the ISM. An increased ISM temperature at higher redshifts is robustly expected based on the temperature of the cosmic microwave background, and also plausibly from higher star formation rates (SFR) which result in more supernova heat input, and lower metallicities, which result in less efficient cooling.

An evolving IMF, in which the characteristic mass increases with increasing redshift, provides an explanation for a number of discrepancies: The difference in evolution of dynamical  $M/L$  ratios and colors of early-type galaxies (van Dokkum 2008); The difference in evolution of the galaxy SFR - stellar mass relation between  $\Lambda$ CDM galaxy formation models and observations (Davé 2008); The difference between the observed stellar mass density of the universe and the implied stellar mass density from integrating the cosmic star formation history (Larson 2005; Hopkins & Beacom 2006; Fardal et al. 2007).

As shown by van Dokkum (2008), for IMFs with  $m_c < 0.08$  (i.e., more bottom heavy than a Chabrier IMF), the stellar  $M/L$  ratios increase for decreasing  $m_c$ . For  $m_c > 0.08$  (i.e., more bottom light than a Chabrier IMF) the stellar  $M/L$  ratio decreases. However, the relation between stellar  $M/L$  and  $m_c$  is not monotonic. As  $m_c$  increases beyond  $\sim 0.3M_{\odot}$  the stellar  $M/L$  can actually *increase*. This is because the mass function becomes dominated by stellar remnants. For old enough stellar populations (Age  $\sim 5 - 10$  Gyr) with  $m_c \sim 1$  the stellar  $M/L$  can equal or even exceed that of a Salpeter IMF.

Since ETGs form their stars at higher redshifts than

LTGs, the evolving IMF as proposed by Van Dokkum (2008) and Davé (2008) would cause ETGs to have higher present day stellar  $M/L$  ratios than LTGs. The normalizations of the  $M/L$  ratios are expected to be Salpeter like for ETGs, and not lower than 0.1 dex below Chabrier for LTGs (van Dokkum 2008). In the context of our results, stellar  $M/L$  ratios close to Salpeter for ETGs are inconsistent with halo contraction. If the IMF for LTGs is close to Chabrier, then this would also favor models with halo expansion or no halo contraction. Thus this evolving IMF requires that the haloes of both ETGs and LTGs do not contract in response to galaxy formation.

Recently van Dokkum & Conroy (2010) derived constraints on the stellar IMF in the cores of massive elliptical galaxies using stellar absorption lines in the near-IR. They find strong evidence for an IMF with a steeper low mass slope than a Salpeter IMF, i.e., a bottom-heavy IMF. If the IMF is bottom-heavy throughout massive elliptical galaxies, and not just in their centers, then this is the opposite result to what is expected from the evolving IMF models of van Dokkum (2008) and Davé (2008).

This bottom heavy IMF results in stellar  $M/L$  ratios a factor of  $\sim 1.4$  higher than a regular Salpeter IMF. As shown in Fig. 12 the dark matter fractions within the effective radii for the most massive early-type galaxies are  $\sim 0.3$  for a Salpeter IMF. Thus, given the current uncertainties in  $V_c/\sigma_e$ , the IMF from van Dokkum & Conroy (2010) is permitted to apply globally in massive early-type galaxies, and not just in their centers. However, this IMF would strongly over-predict the total masses within the effective radii of intermediate mass ( $M_{\text{star}} \sim 10^{10}M_{\odot}$ ) early-type galaxies. Thus based on our mass models we do not expect the bottom-heavy IMF of van Dokkum & Conroy (2010) to be universal across early-type galaxies of different masses.

## 5.3 Comparison with previous studies

There are several recent studies that have addressed dark halo contraction and the stellar initial mass function of galaxies (Treu et al. 2010; Schulz et al. 2010; Trujillo-Gomez et al. 2010; Auger et al. 2010a; Napolitano et al. 2010). Most of these have focused on massive early-type galaxies. Although the individual conclusions vary, all of them are consistent with the following: ETGs with a Chabrier IMF plus un-contracted NFW haloes with standard halo concentrations do not have enough mass within the effective radius.

Schulz et al. (2010) and Trujillo-Gomez et al. (2010) advocate models with halo contraction (Gnedin et al. 2004, and Blumenthal et al. 1986, respectively) to provide this additional mass, whereas Treu et al. (2010) and Auger et al. (2010a) advocate a Salpeter IMF. Schulz et al. (2010) argue against a Salpeter IMF based on the results of Cappellari et al. (2006). However, there are some caveats to this line of reasoning. Firstly the dynamical masses from Cappellari et al. (2006) are consistent with a Salpeter IMF for the most massive galaxies. Secondly the dynamical masses from Cappellari et al. (2006) assume mass follows light, which is expected to result in an underestimate of the dynamical masses if the dark matter fractions within the effective radii are significant. In §3.7 we showed that the Cappellari et al. (2006) dynamical masses imply that, on average,  $V_c/\sigma_e = 1.44 \pm 0.01$ . In Fig. 12 we showed that if  $V_c/\sigma_e \gtrsim 1.6$

then a Salpeter IMF is consistent for ETGs of all masses. Thus a Salpeter IMF is allowed for the most massive ETGs, and it is not yet robustly ruled out for intermediate mass ETGs (where the dark matter fractions are expected to be the lowest).

Auger et al. (2010a) combined strong lensing, weak lensing and stellar dynamics for a sample of 53 massive elliptical galaxies to place constraints on the stellar IMF. They conclude that, given their model assumptions, the data strongly prefer a Salpeter like IMF over a lighter IMF such as Chabrier or Kroupa. While we agree that a model with a Salpeter like IMF can reproduce the observations, we find that our data cannot distinguish between models with Salpeter and Chabrier IMFs. Below we discuss two areas that could contribute to these differences: anisotropy and halo masses.

The use of strong lensing and stellar dynamics can constrain the slope of the total mass profile within an effective radius (e.g., Koopmans et al. 2006). As we show in § 4.2 this information can help distinguish between models with different IMFs. However, a major source of systematic uncertainty is the anisotropy of the stellar orbits (Koopmans et al. 2009). Auger et al. (2010a) assumed isotropic orbits,  $\beta = 0$ , and thus may have inadvertently favoured a particular IMF.

In order to constrain the halo contraction model the halo mass needs to be accurately determined. This is for 2 reasons. Firstly, the halo mass is needed to predict the typical pristine halo concentration using cosmological N-body simulations. Secondly, to provide an accurate normalization of the halo mass profile. For a fixed IMF, the relation between stellar mass and halo mass has been determined using halo abundance matching, weak lensing and satellite kinematics. These techniques yield consistent results, and in particular for massive early-type galaxies (Dutton et al. 2010b; More et al. 2011), and thus provide a consistency check on the models of Auger et al. (2010a). Taking a model with a Chabrier IMF and Gnedin et al. (2004) halo contraction, Auger et al. (2010a) find halo masses a factor of  $\sim 0.5$  dex lower than obtained by Moster et al. (2010). The relation from Moster et al. (2010) is in good agreement with the relations we use in this paper for massive early-type galaxies (see Fig. 1 in Dutton et al. 2010b). Thus Auger et al. (2010a) is inferring abnormally low halo masses at fixed stellar mass, which may be biasing their results (as previously discussed by Tortora et al. 2010).

Schulz et al. (2010) argue that the halo contraction models of Abadi et al. (2010) and Blumenthal et al. (1986) are inconsistent with the data. We disagree with this conclusion, as we show that for a Chabrier IMF, all three halo contraction models are consistent with the data, given reasonable systematic uncertainties. Furthermore, distinguishing between the Gnedin et al. (2004) and Abadi et al. (2010) models requires stellar masses to be measured to an accuracy of 0.1 dex. Such accuracy may in principle be achievable for early-type galaxies (Gallazzi & Bell 2009), but the current limiting factors are uncertainties in stellar population synthesis models (Conroy, Gunn, & White 2009).

The degeneracy between halo contraction and stellar IMF for early-types was also discussed by Napolitano et al. (2010), with similar qualitative conclusions as we find here. However, a limitation of this study was the treatment

of the stellar mass to halo mass ratio as a free parameter. In our analysis the halo masses are constrained through results from weak lensing and satellite kinematics, which enables us to make more quantitative conclusions regarding the nature of dark halo response for a given IMF. Finally, we note that the conclusion of Napolitano et al. (2010) that the relation between the central dark matter density and effective radius provides evidence for cuspy dark matter haloes is in fact degenerate with the IMF.

Our conclusions for late-type galaxies are in agreement with those of Dutton et al. (2007), namely that for a Chabrier IMF, halo expansion is required to match the zero point of the TF relation (as well as galaxy sizes). Trujillo-Gomez et al. (2010) claim their results are incompatible with the conclusions of Dutton et al. (2007). However, their figures show that a model with Blumenthal et al. (1986) adiabatic halo contraction is consistent with the velocity-luminosity (VL) relation of early-types, but it does not match the VL relation of late-types. Their model without halo contraction provides a better fit to the VL relation of late-types. Their results are thus consistent with our findings.

#### 5.4 Future prospects

There are a number of techniques that are capable of constraining the IMF and/or dark matter fractions in galaxies. Here we give a brief outline of these.

Upper limits to stellar  $M/L$  ratios are obtainable from both strong lensing and dynamical models. The strongest constraints are expected for intermediate mass early-type galaxies, as these are expected to have the highest baryon fractions within the effective radius (Fig. 12). The ATLAS3D project (Cappellari et al. 2011) contains  $\sim 10$  times more galaxies than studied by Cappellari et al. (2006), and thus promises to provide stronger constraints on  $V_{\text{circ}}(R_e)/\sigma_e$  over a wider range of galaxy masses than previous dynamical studies. Strong lensing has the potential to provide stronger constraints than dynamical models, but it is currently limited by the sparsity of known strong lenses with  $M_{\text{star}} \sim 10^{10} M_{\odot}$ . Furthermore, low mass early-type galaxies tend to be satellites, which adds an extra complication to inferring total masses from strong lensing. Strong lensing will be able measure the total projected mass accurately, but the problem will be disentangling the mass of the satellite from that of its host.

There is a well known disk-halo degeneracy that plagues the decomposition of galaxy rotation curves into baryonic and dark matter components (e.g., van Albada & Sancisi 1986; van den Bosch & Swaters 2001; Dutton et al. 2005). Strong gravitational lensing of high inclination disk-dominated galaxies can provide a complementary information to that obtainable from kinematics. Specifically, strong lensing measures projected mass, and ellipticity of projected mass. Both of which depend on the disk mass fraction, and thus a combined strong lensing and dynamics analysis can place constraints on the stellar  $M/L$  ratio (Dutton et al. 2011, in prep). This technique has not been fully exploited due to the lack of known disk dominated strong lenses. However, searches for spiral galaxy strong lenses are underway (Féron et al. 2009; Sygnet et al. 2010;

Treu et al. 2011, in prep), and thus the primary limitation of this method will be soon overcome.

An absolute constraint on disk masses can be obtained by using the fact that the disk surface mass density is a function of the vertical velocity dispersion and the disk scale height (Bottema 1993). This method is being applied by the Disk Mass Survey (Verheijen et al. 2007; Bershadsky et al. 2010). They are measuring the disk mass density profile from vertical velocity dispersions and a statistical measurement of disk scale heights. By subtracting off the observed gas mass density this gives the stellar mass density profile. This method is limited to regions of galaxies where the disk dominates the baryons, i.e., it does not apply to elliptical galaxies or the bulges of spiral galaxies. It is also a statistical method, since it requires knowledge of two parameters that cannot be measured simultaneously.

Constraints on dark matter fractions can be obtained from the scatter in the velocity-mass (VM) and size-mass (RM) relations. The basic idea is that the strength of correlation between residuals of the VM and RM relations depends on the dark matter fraction. This method has been applied to late-type galaxies (Courteau & Rix 1999; Dutton et al. 2007; Gnedin et al. 2007), but the interpretation in terms of dark matter fractions are not always unique. We plan to apply this method to early-type galaxies in a future paper (Dutton et al. 2011, in prep.)

The low-mass end of the IMF can be constrained with stellar absorption lines (van Dokkum & Conroy 2010). The lines are weak and at  $\sim 900$  nm, so that this method is only applicable to non-star forming galaxies. The galaxy redshifts are currently limited to be very low by detector technology. This method has only currently been applied to the centers of massive early-type galaxies, with evidence for an IMF more bottom heavy than Salpeter. It would be very interesting to see this method applied radially and in lower mass early-types.

## 6 SUMMARY

We use structural and dynamical scaling relations of early-type galaxies (ETGs) and late-type galaxies (LTGs) to place constraints on the stellar initial mass function (IMF) and dark halo response to galaxy formation, which is commonly modeled as adiabatic contraction (AC). We build bulge-disk-halo models that by construction reproduce the observed structural scaling relations of galaxies: optical size vs stellar mass; bulge fraction vs stellar mass; gas mass vs stellar mass; and gas size vs stellar mass. The dark matter haloes are constrained to reproduce the observed halo mass vs stellar mass relation from satellite kinematics and weak lensing (Dutton et al. 2010b), and the concentration - halo mass relation from cosmological N-body simulations (Macciò et al. 2008). Lastly, the Tully-Fisher (TF) and Faber-Jackson (FJ) relations provide a constraint on the total mass within 2.2 disk scale lengths for LTGs and the half-light radius,  $R_e$ , for ETGs.

A key uncertainty in the constraint from the FJ relation is the conversion between the observed stellar velocity dispersion within the half-light radius,  $\sigma(< R_e) \equiv \sigma_e$ , and the circular velocity within the half-light radius,  $V_{\text{circ}}(R_e) \equiv V_c$ . Using results from the SLACS survey we show that for

massive early-type galaxies ( $M_{\text{star}} > 10^{11} M_{\odot}$ ), on average  $V_c/\sigma_e = 1.54 \pm 0.02$ . We show that the SAURON results from Cappellari et al. (2006), which make use of a smaller sample, but cover a much larger range in stellar mass  $3 \times 10^9 - 4 \times 10^{11} M_{\odot}$ , imply that on average  $V_c/\sigma_e = 1.44 \pm 0.01$ . The inconsistency of these two results implies that there are systematic effects which bias either or both of these results.

Based on the observed scaling relations alone, we calculate the spherical dark matter fraction within the half-light radius for ETGs and 2.2 disk scale lengths for LTGs. For LTGs the dark matter fraction increases with increasing stellar mass (in agreement with previous studies), while for ETGs the dark matter fraction reaches a minimum for a stellar mass of  $M_{\text{star}} \sim 10^{10} M_{\odot}$  (Assuming a Chabrier IMF), and velocity dispersions of  $\sigma_e \sim 100 \text{ km s}^{-1}$ . The dark matter fraction increases towards both lower and higher masses.

High mass ETGs are consistent with a Salpeter IMF (i.e., the stellar mass fraction implied by the structural scaling relations is less than the dynamically inferred mass.) However, a Salpeter IMF is ruled out for galaxies with velocity dispersions  $\sigma_e \sim 100 \text{ km s}^{-1}$ , unless  $V_c/\sigma_e \gtrsim 1.6$ . Thus improved constraints on  $V_c/\sigma_e$  for intermediate mass ETGs from strong lensing or dynamical modeling would provide the strongest upper limits to the IMF.

Our bulge-disk-halo models reproduce the slopes of the FJ and TF relations, for ETGs and LTGs respectively. However, models with a universal IMF and universal halo response to galaxy formation are unable to *simultaneously* match the zero points of the FJ and TF relations. For a given AC model, ETGs require higher stellar mass normalizations (i.e., IMFs with higher stellar mass-to-light ratios) than LTGs. For a given IMF, ETGs require stronger halo contraction.

For early-type galaxies, models with a Chabrier IMF and adiabatic contraction according to Gnedin et al. (2004) provide good fits to the FJ relation. Models with adiabatic contraction according to Blumenthal et al. (1986) and Abadi et al. (2010) also provide good fits, within the systematic uncertainties in dark halo masses and  $V_c/\sigma_e$ . Distinguishing between the models of Gnedin et al. (2004) and Abadi et al. (2010), and hence constraining the stability of AC to bombardment from major and minor mergers, requires measuring stellar masses to within 0.1 dex, which seems beyond the reach of current SPS models. Models without adiabatic contraction favor an IMF  $\simeq 0.17$  dex heavier than Chabrier.

For late-type galaxies, models with adiabatic contraction require lighter IMFs (i.e., lower stellar mass-to-light ratios) than Chabrier (at least 0.10 dex for Abadi et al. 2010, 0.20 dex for Gnedin et al. 2004, and 0.25 dex for Blumenthal et al. 1986). Matching the TF relation with a Chabrier IMF requires mild halo expansion, in agreement with Dutton et al. (2007). Producing stellar masses lower by  $\sim 0.3$  dex is not possible from plausible variations in the IMF, and thus lower stellar masses would need to arise from systematic uncertainties in stellar population synthesis models or the application of these models in deriving stellar masses.

Evolution of the IMF as proposed by van Dokkum (2008) and Davé (2008) would cause ETGs to have higher present day stellar  $M/L$  than LTGs. The normalization for ETGs would be significantly higher than Chabrier, and thus disfavoring dark halo contraction.



Alternatively, if the IMF is universal, we envision the following scenario which results in halo expansion in late-types and halo contraction in early-types. We suppose that the distinguishing feature between ETGs and LTGs is that ETGs assemble a significant fraction of their stellar mass in major merger events. For galaxies without a major mergers, the dark haloes expand due to a combination of dynamical friction from baryonic clumps during the early phases of galaxy formation (El-Zant et al. 2001; Mashchenko et al. 2006; Elmegreen et al. 2008) and/or supernova/stellar wind driven mass outflows (Navarro et al. 1996b; Read & Gilmore 2005; Governato et al. 2010). These galaxies will become late-types (star forming and disk dominated). When galaxies experience a major dissipative merger, large amounts of gas accumulate at the center of the remnant, resulting in standard halo contraction (i.e., Gnedin et al. 2004). Subsequent bombardment from non-dissipative mergers may reduce the amount of halo contraction (Johansson et al. 2009; Abadi et al. 2010). A prediction of this scenario would be that bulge dominated LTGs should have more contraction than disk dominated LTGs of the same overall mass.

Finally we show that our models naturally reproduce flat and featureless circular velocity profiles within the optical regions of both early and late-type galaxies for a wide range of halo responses (including contraction and expansion) and IMFs.

## ACKNOWLEDGMENTS

A.A.D. acknowledges financial support from the Canadian Institute for Theoretical Astrophysics (CITA) National Fellows program. S.C. acknowledges the support of a Discovery grant by the Natural Science and Engineering Research Council of Canada. The work of A.D. was partly supported by ISF grant 6/08, by GIF grant G-1052-104.7/2009, by a DIP grant, by the Einstein Center at HU, and by NSF grant 1010033 at UCSC. This research has made use of NASA's Astrophysics Data System Bibliographic Services.

Funding for the Sloan Digital Sky Survey (SDSS) has been provided by the Alfred P. Sloan Foundation, the Participating Institutions, the National Aeronautics and Space Administration, the National Science Foundation, the U.S. Department of Energy, the Japanese Monbukagakusho, and the Max Planck Society. The SDSS Web site is <http://www.sdss.org/>.

The SDSS is managed by the Astrophysical Research Consortium (ARC) for the Participating Institutions. The Participating Institutions are The University of Chicago, Fermilab, the Institute for Advanced Study, the Japan Participation Group, The Johns Hopkins University, Los Alamos National Laboratory, the Max-Planck-Institute for Astronomy (MPIA), the Max-Planck-Institute for Astrophysics (MPA), New Mexico State University, University of Pittsburgh, Princeton University, the United States Naval Observatory, and the University of Washington.

## REFERENCES

Abazajian, K. N., et al. 2009, *ApJS*, 182, 543

- Abadi, M. G., Navarro, J. F., Fardal, M., Babul, A., & Steinmetz, M. 2010, *MNRAS*, 407, 435
- Auger, M. W., Treu, T., Bolton, A. S., Gavazzi, R., Koopmans, L. V. E., Marshall, P. J., Bundy, K., & Moustakas, L. A. 2009, *ApJ*, 705, 1099
- Auger, M. W., Treu, T., Gavazzi, R., Bolton, A. S., Koopmans, L. V. E., & Marshall, P. J. 2010a, *ApJL*, 721, L163
- Auger, M. W., Treu, T., Bolton, A. S., Gavazzi, R., Koopmans, L. V. E., Marshall, P. J., Moustakas, L. A., & Burles, S. 2010b, *ApJ*, 724, 511
- Baldry, I. K., Glazebrook, K., & Driver, S. P. 2008, *MNRAS*, 388, 945
- Barnabe, M., Czoske, O., Koopmans, L. V. E., Treu, T., & Bolton, A. S. 2011, arXiv:1102.2261
- Behroozi, P. S., Conroy, C., & Wechsler, R. H. 2010, *ApJ*, 717, 379
- Bell, E. F., & de Jong, R. S. 2001, *ApJ*, 550, 212
- Bell, E. F., McIntosh, D. H., Katz, N., & Weinberg, M. D. 2003, *ApJS*, 149, 289
- Bernardi, M., Shankar, F., Hyde, J. B., Mei, S., Marulli, F., & Sheth, R. K. 2010, *MNRAS*, 404, 2087
- Bernardi, M., Roche, N., Shankar, F., & Sheth, R. K. 2011, *MNRAS*, 412, L6
- Bershady, M. A., Verheijen, M. A. W., Swaters, R. A., Andersen, D. R., Westfall, K. B., & Martinsson, T. 2010, *ApJ*, 716, 198
- Binney, J., & Tremaine, S. 1987, Princeton, NJ, Princeton University Press, 1987, 747 p.,
- Blanton, M. R., & Roweis, S. 2007, *AJ*, 133, 734
- Bolton, A. S., Burles, S., Koopmans, L. V. E., Treu, T., & Moustakas, L. A. 2006, *ApJ*, 638, 703
- Bolton, A. S., Burles, S., Koopmans, L. V. E., Treu, T., Gavazzi, R., Moustakas, L. A., Wayth, R., & Schlegel, D. J. 2008a, *ApJ*, 682, 964
- Bolton, A. S., Treu, T., Koopmans, L. V. E., Gavazzi, R., Moustakas, L. A., Burles, S., Schlegel, D. J., & Wayth, R. 2008b, *ApJ*, 684, 248
- Bottema, R. 1993, *A&A*, 275, 16
- Bruzual, G., & Charlot, S. 2003, *MNRAS*, 344, 1000
- Blumenthal, G. R., Faber, S. M., Flores, R., & Primack, J. R., 1986, *ApJ*, 301, 27
- Bullock, J. S., Kolatt, T. S., Sigad, Y., Somerville, R. S., Kravtsov, A. V., Klypin, A. A., Primack, J. R., & Dekel, A. 2001, *MNRAS*, 321, 559
- Cappellari, M., et al. 2006, *MNRAS*, 366, 1126
- Cappellari, M., et al. 2011, *MNRAS*, 413, 813
- Catinella, B., et al. 2010, *MNRAS*, 403, 683
- Chabrier, G. 2003, *PASP*, 115, 763
- Courteau, S., de Jong, R. S., & Broeils, A. H. 1996, *ApJL*, 457, L73
- Courteau, S., & Rix, H. 1999, *ApJ*, 513, 561
- Courteau, S., McDonald, M., Widrow, L. M., & Holtzman, J. 2007a, *ApJL*, 655, L21
- Courteau, S., Dutton, A. A., van den Bosch, F. C., MacArthur, L. A., Dekel, A., McIntosh, D. H., & Dale, D. A. 2007b, *ApJ*, 671, 203
- Conroy, C., et al. 2007, *ApJ*, 654, 153
- Conroy, C., Gunn, J. E., & White, M. 2009, *ApJ*, 699, 486
- Dalcanton, J. J., & Stilp, A. M. 2010, *ApJ*, 721, 547
- Davé, R. 2008, *MNRAS*, 385, 147
- Davies, R. L., Efsthathiou, G., Fall, S. M., Illingworth, G., & Schechter, P. L. 1983, *ApJ*, 266, 41
- Dekel, A., & Cox, T. J. 2006, *MNRAS*, 370, 1445
- Dekel, A., et al. 2009, *Nature*, 457, 451
- Diemand, J., Zemp, M., Moore, B., Stadel, J., & Carollo, C. M. 2005, *MNRAS*, 364, 665
- Diemand, J., Kuhlen, M., & Madau, P. 2007, *ApJ*, 667, 859
- Djorgovski, S., & Davis, M. 1987, *ApJ*, 313, 59
- Dobke, B. M., & King, L. J. 2006, *A&A*, 460, 647

- Dressler, A., Lynden-Bell, D., Burstein, D., Davies, R. L., Faber, S. M., Terlevich, R., & Wegner, G. 1987, *ApJ*, 313, 42
- Duffy, A. R., Schaye, J., Kay, S. T., Dalla Vecchia, C., Battye, R. A., & Booth, C. M. 2010, *MNRAS*, 405, 2161
- Dutton, A. A., Courteau, S., de Jong, R., & Carignan, C. 2005, *ApJ*, 619, 218
- Dutton, A. A., van den Bosch, F. C., Dekel, A., & Courteau, S. 2007, *ApJ*, 654, 27
- Dutton, A. A., van den Bosch, F. C., & Courteau, S. 2008, *Astronomical Society of the Pacific Conference Series*, 396, 467
- Dutton, A. A. 2009, *MNRAS*, 396, 121
- Dutton, A. A., & van den Bosch, F. C. 2009, *MNRAS*, 396, 141
- Dutton, A. A., van den Bosch, F. C., & Dekel, A. 2010a, *MNRAS*, 405, 1690
- Dutton, A. A., Conroy, C., van den Bosch, F. C., Prada, F., & More, S. 2010b, *MNRAS*, 407, 2
- Dutton, A. A., et al. 2011, *MNRAS*, 410, 1660
- Dunkley, J., et al. 2009, *ApJS*, 180, 306
- Eke, V. R., Navarro, J. F., & Steinmetz, M. 2001, *ApJ*, 554, 114
- Elmegreen, B. G., Bournaud, F., & Elmegreen, D. M. 2008, *ApJ*, 688, 67
- El-Zant, A. A., Shlosman, I., & Hoffman, Y. 2001, *ApJ*, 560, 636
- El-Zant, A. A., Hoffman, Y., Primack, J., Combes, F., & Shlosman, I. 2004, *ApJL*, 607, L75
- Faber, S. M., & Jackson, R. E. 1976, *ApJ*, 204, 668
- Fardal, M. A., Katz, N., Weinberg, D. H., & Davé, R. 2007, *MNRAS*, 379, 985
- Féron, C., Hjorth, J., McKean, J. P., & Samsing, J. 2009, *ApJ*, 696, 1319
- Ferrarese, L., et al. 2006, *ApJS*, 164, 334
- Freeman, K. C. 1970, *ApJ*, 160, 811
- Gallazzi, A., Charlot, S., Brinchmann, J., & White, S. D. M. 2006, *MNRAS*, 370, 1106
- Gallazzi, A., & Bell, E. F. 2009, *ApJS*, 185, 253
- Garnett, D. R. 2002, *ApJ*, 581, 1019
- Geha, M., Blanton, M. R., Masjedi, M., & West, A. A. 2006, *ApJ*, 653, 240
- Gnedin, O. Y., & Zhao, H. 2002, *MNRAS*, 333, 299
- Gnedin, O. Y., Kravtsov, A. V., Klypin, A. A., & Nagai, D. 2004, *ApJ*, 616, 16
- Governato, F., et al. 2010, *Nature*, 463, 203
- Graham, A. W., & Guzmán, R. 2003, *AJ*, 125, 2936
- Graham, A. W., & Worley, C. C. 2008, *MNRAS*, 388, 1708
- Guo, Q., White, S., Li, C., & Boylan-Kolchin, M. 2010, *MNRAS*, 404, 1111
- Hernquist, L. 1990, *ApJ*, 356, 359
- Holley-Bockelmann, K., Weinberg, M., & Katz, N. 2005, *MNRAS*, 363, 991
- Hopkins, A. M., & Beacom, J. F. 2006, *ApJ*, 651, 142
- Hopkins, P. F., Cox, T. J., & Hernquist, L. 2008, *ApJ*, 689, 17
- Hopkins, P. F., Cox, T. J., Younger, J. D., & Hernquist, L. 2009a, *ApJ*, 691, 1168
- Hopkins, P. F., et al. 2009b, *MNRAS*, 397, 802
- Hyde, J. B., & Bernardi, M. 2009, *MNRAS*, 396, 1171
- Jardel, J. R., & Sellwood, J. A. 2009, *ApJ*, 691, 1300
- Jing, Y. P. 2000, *ApJ*, 535, 30
- Johansson, P. H., Naab, T., & Ostriker, J. P. 2009, *ApJL*, 697, L38
- Jorgensen, I., Franx, M., & Kjaergaard, P. 1995, *MNRAS*, 276, 1341
- Kannappan, S. J. 2004, *ApJL*, 611, L89
- Klypin, A., Zhao, H., & Somerville, R. S. 2002, *ApJ*, 573, 597
- Klypin, A., Trujillo-Gomez, S., & Primack, J. 2010, *arXiv:1002.3660*
- Komatsu, E., et al. 2009, *ApJS*, 180, 330
- Koopmans, L. V. E., Treu, T., Bolton, A. S., Burles, S., & Moustakas, L. A. 2006, *ApJ*, 649, 599
- Koopmans, L. V. E., et al. 2009, *ApJL*, 703, L51
- Kormendy, J., Fisher, D. B., Cornell, M. E., & Bender, R. 2009, *ApJS*, 182, 216
- Kroupa, P. 2001, *MNRAS*, 322, 231
- Larson, R. B. 1998, *MNRAS*, 301, 569
- Larson, R. B. 2005, *The Initial Mass Function 50 Years Later*, 327, 329
- Leroy, A. K., Walter, F., Brinks, E., Bigiel, F., de Blok, W. J. G., Madore, B., & Thornley, M. D. 2008, *AJ*, 136, 2782
- Li, C., & White, S. D. M. 2009, *MNRAS*, 398, 2177
- MacArthur, L. A., Courteau, S., & Holtzman, J. A. 2003, *ApJ*, 582, 689
- Macciò, A. V., Dutton, A. A., van den Bosch, F. C., Moore, B., Potter, D., & Stadel, J. 2007, *MNRAS*, 378, 55
- Macciò, A. V., Dutton, A. A., & van den Bosch, F. C. 2008, *MNRAS*, 391, 1940
- Maller, A. H. 2008, *Astronomical Society of the Pacific Conference Series*, 396, 251
- Mandelbaum, R., Seljak, U., Kauffmann, G., Hirata, C. M., & Brinkmann, J. 2006, *MNRAS*, 368, 715
- Mashchenko, S., Couchman, H. M. P., & Wadsley, J. 2006, *Nature*, 442, 539
- Mashchenko, S., Wadsley, J., & Couchman, H. M. P. 2008, *Science*, 319, 174
- Matković, A., & Guzmán, R. 2005, *MNRAS*, 362, 289
- McGaugh, S. S., & de Blok, W. J. G. 1997, *ApJ*, 481, 689
- McGaugh, S. S. 2005, *ApJ*, 632, 859
- McDonald, M., Courteau, S., & Tully, R. B. 2009, *MNRAS*, 393, 628
- Merritt, D., Graham, A. W., Moore, B., Diemand, J., & Terzić, B. 2006, *AJ*, 132, 2685
- Mo, H. J., & Mao, S. 2004, *MNRAS*, 353, 829
- More, S., van den Bosch, F. C., Cacciato, M., Skibba, R., Mo, H. J., & Yang, X. 2011, *MNRAS*, 410, 210
- Moster, B. P., Somerville, R. S., Maulbetsch, C., van den Bosch, F. C., Macciò, A. V., Naab, T., & Oser, L. 2010, *ApJ*, 710, 903
- Muñoz-Cuartas, J. C., Macciò, A. V., Gottlöber, S., & Dutton, A. A. 2011, *MNRAS*, 411, 584
- Napolitano, N. R., Romanowsky, A. J., & Tortora, C. 2010, *MNRAS*, 405, 2351
- Navarro, J. F., Frenk, C. S., & White, S. D. M. 1996a, *ApJ*, 462, 563
- Navarro, J. F., Eke, V. R., & Frenk, C. S. 1996b, *MNRAS*, 283, L72
- Navarro, J. F., Frenk, C. S., & White, S. D. M. 1997, *ApJ*, 490, 493
- Navarro, J. F., et al. 2004, *MNRAS*, 349, 1039
- Navarro, J. F., et al. 2010, *MNRAS*, 402, 21
- Neistein, E., Li, C., Khochfar, S., Weinmann, S. M., Shankar, F., & Boylan-Kolchin, M. 2011, *arXiv:1103.3272*
- Neto, A. F., et al. 2007, *MNRAS*, 381, 1450
- Noordermeer, E., & Verheijen, M. A. W. 2007, *MNRAS*, 381, 1463
- Padmanabhan, N., et al. 2004, *New Astronomy*, 9, 329
- Pedrosa, S., Tissera, P. B., & Scannapieco, C. 2010, *MNRAS*, 402, 776
- Fioc, M., & Rocca-Volmerange, B. 1997, *A&A*, 326, 950
- Pizagno, J., et al. 2005, *ApJ*, 633, 844
- Pizagno, J., et al. 2007, *AJ*, 134, 945
- Portinari, L., Sommer-Larsen, J., & Tantalo, R. 2004, *MNRAS*, 347, 691
- Prugniel, P., & Simien, F. 1997, *A&A*, 321, 111
- Read, J. I., & Gilmore, G. 2005, *MNRAS*, 356, 107
- Romano-Díaz, E., Shlosman, I., Hoffman, Y., & Heller, C. 2008, *ApJL*, 685, L105
- Salpeter, E. E. 1955, *ApJ*, 121, 161
- Schulz, A. E., Mandelbaum, R., & Padmanabhan, N. 2010, *MNRAS*, 408, 1463

- Sellwood, J. A., & McGaugh, S. S. 2005, *ApJ*, 634, 70
- Sellwood, J. A. 2008, *ApJ*, 679, 379
- Shen, S., Mo, H. J., White, S. D. M., Blanton, M. R., Kauffmann, G., Voges, W., Brinkmann, J., & Csabai, I. 2003, *MNRAS*, 343, 978
- Simard, L., et al. 2002, *ApJS*, 142, 1
- Stark, D. V., McGaugh, S. S., & Swaters, R. A. 2009, *AJ*, 138, 392
- Swaters, R. A. 1999, Ph.D. Thesis
- Sygnnet, J. F., Tu, H., Fort, B., & Gavazzi, R. 2010, *A&A*, 517, A25
- Tissera, P. B., White, S. D. M., Pedrosa, S., & Scannapieco, C. 2010, *MNRAS*, 406, 922
- Tollerud, E. J., Bullock, J. S., Graves, G. J., & Wolf, J. 2011, *ApJ*, 726, 108
- Tonry, J. L. 1981, *ApJL*, 251, L1
- Toomre, A., & Toomre, J. 1972, *ApJ*, 178, 623
- Tortora, C., Napolitano, N. R., Romanowsky, A. J., Capaccioli, M., & Covone, G. 2009, *MNRAS*, 396, 1132
- Tortora, C., Napolitano, N. R., Romanowsky, A. J., & Jetzer, P. 2010, *ApJL*, 721, L1
- Treu, T., Auger, M. W., Koopmans, L. V. E., Gavazzi, R., Marshall, P. J., & Bolton, A. S. 2010, *ApJ*, 709, 1195
- Trujillo-Gomez, S., Klypin, A., Primack, J., & Romanowsky, A. J. 2010, arXiv:1005.1289
- Tully, R. B., & Fisher, J. R. 1977, *A&A*, 54, 661
- van Albada, T. S., & Sancisi, R. 1986, *Royal Society of London Philosophical Transactions Series A*, 320, 447
- van den Bosch, F. C., & de Zeeuw, P. T. 1996, *MNRAS*, 283, 381
- van den Bosch, F. C., & Swaters, R. A. 2001, *MNRAS*, 325, 1017
- van den Bosch, F. C., Aquino, D., Yang, X., Mo, H. J., Pasquali, A., McIntosh, D. H., Weinmann, S. M., & Kang, X. 2008, *MNRAS*, 387, 79
- van Dokkum, P. G. 2008, *ApJ*, 674, 29
- van Dokkum, P. G., & Conroy, C. 2010, *Nature*, 468, 940
- Verheijen, M. A. W. 2001, *ApJ*, 563, 694 [V01]
- Verheijen, M. A. W., Bershady, M. A., Swaters, R. A., Andersen, D. R., & Westfall, K. B. 2007, *Island Universes - Structure and Evolution of Disk Galaxies*, 95
- Wechsler, R. H., Bullock, J. S., Primack, J. R., Kravtsov, A. V., & Dekel, A. 2002, *ApJ*, 568, 52
- Weinberg, M. D., & Katz, N. 2002, *ApJ*, 580, 627
- Wilson, G. M. 2003, PhD Thesis, The Australian National University
- Williams, M. J., Bureau, M., & Cappellari, M. 2010, *MNRAS*, 409, 1330
- Wolf, J., Martinez, G. D., Bullock, J. S., Kaplinghat, M., Geha, M., Muñoz, R. R., Simon, J. D., & Avedo, F. F. 2010, *MNRAS*, 406, 1220
- York, D. G., et al. 2000, *AJ*, 120, 1579
- Yang, X., Mo, H. J., & van den Bosch, F. C. 2008, *ApJ*, 676, 248
- Yang, X., Mo, H. J., & van den Bosch, F. C. 2009, *ApJ*, 695, 900
- Zhao, D. H., Mo, H. J., Jing, Y. P., Börner, G. 2003, *MNRAS*, 339, 12
- Zhao, D. H., Jing, Y. P., Mo, H. J., Börner, G. 2009, *ApJ*, 707, 354
- Zwaan, M. A., van der Hulst, J. M., de Blok, W. J. G., & McGaugh, S. S. 1995, *MNRAS*, 273, L35